Cell competition with normal epithelial cells promotes apical extrusion of transformed cells through metabolic changes

Shunsuke Kon[1*], Kojiro Ishibashi[1*], Hiroto Katoh[1], Sho Kitamoto[1], Takanobu Shirai[1], Shinya Tanaka[1], Mihoko Kajita[1], Susumu Ishikawa[1], Hajime Yamauchi[1], Yuta Yako[1], Tomoko Kamasaki[1], Tomohiro Matsumoto[1], Hirotaka Watanabe[1], Riku Egami[1], Ayana Sasaki[1], Atsuko Nishikawa[1], Ikumi Kameda[1], Takeshi Maruyama[1], Rika Narumi[1], Tomoko Morita[1], Yoshiteru Sasaki[2], Ryosuke Enoki[3,4,5], Sato Honma[4], Hiromi Imamura[6], Masanobu Oshima[7], Tomoyoshi Soga[8], Jun-ichi Miyazaki[9], Michael R Duchen[10], Jin-Min Nam[11], Yasuhito Onodera[12], Shingo Yoshioka[13], Junichi Kikuta[13], Masaru Ishii[13], Masamichi Imajo[14], Eisuke Nishida[15], Yoichiro Fujioka[16], Yusuke Ohba[16], Toshiro Sato[17] & Yasuyuki Fujita[1]

[1]Division of Molecular Oncology, Institute for Genetic Medicine, Hokkaido University Graduate School of Chemical Sciences and Engineering, Sapporo 060-0815, Japan.

[2]Department of Molecular and Cellular Physiology, Graduate School of Medicine, Kyoto University, Kyoto 606-8501, Japan.

[3]Photonic Bioimaging Section, Research Center for Cooperative projects, Hokkaido University Graduate School of Medicine, Sapporo 060-8638, Japan.

[4]Department of Chronomedicine, Hokkaido University Graduate School of Medicine, Sapporo 060-0810, Japan.

[5]Precursory Research for Embryonic Science and Technology (PRESTO), Japan, Science and Technology Agency (JST), Saitama 332-0012, Japan.

[6]Laboratory of Functional Biology, Graduate School of Biostudies, Kyoto University, Kyoto 606-8501, Japan.

[7]Division of Genetics, Cancer Research Institute, Kanazawa University, Kanazawa 920-1192, Japan.

[8]Institute for Advanced Biosciences, Keio University, Tsuruoka 997-0052, Japan.

[9]Department of Nutrition and Physiological Chemistry, Osaka University Medical School, Osaka 565-0871, Japan.

[10]Research Department of Cell & Developmental Biology, University College London, London WC1E 6BT, UK.

[11]Global Station for Quantum Medical Science and Engineering, Global Institution for Collaborative Research and Education (GI-CoRE), Hokkaido University, Sapporo 060-8648, Japan.

[12]Department of Molecular Biology, Hokkaido University Graduate School of Medicine, Sapporo 060-8638, Japan.

[13]Department of Immunology and Cell Biology, Graduate School of Medicine and Frontier Biosciences, Osaka University, Osaka 565-0871, Japan.

[14]Laboratory of Bioimaging and Cell Signaling, Graduate School of Biostudies, Kyoto University, Kyoto 606-8315, Japan.

[15]Department of Cell and Developmental Biology, Graduate School of Biostudies, Kyoto University, Kyoto 606-8502, Japan.

[16]Department of Cell Physiology, Hokkaido University Graduate School of Medicine, Sapporo 060-8638, Japan.

[17]Department of Gastroenterology, Keio University School of Medicine, Tokyo 160-0016, Japan.

*These authors contributed equally to this work.

ABSTRACT

Recent studies have revealed that newly emerging transformed cells are often apically extruded from epithelial tissues. During this process, normal epithelial cells can recognize and actively eliminate transformed cells, a process called Epithelial Defence Against Cancer (EDAC). Here, we show that mitochondrial membrane potential is diminished in RasV12-transformed cells when they are surrounded by normal cells. In addition, glucose-uptake is elevated, leading to higher lactate production. The mitochondrial dysfunction is driven by upregulation of pyruvate dehydrogenase kinase 4, which positively regulates elimination of RasV12-transformed cells. Furthermore, EDAC from the surrounding normal cells, involving Filamin, drives the Warburg effect-like metabolic alteration. Moreover, using the novel cell competition mouse model, we demonstrate that PDK-mediated metabolic changes promote the elimination of RasV12-transformed cells from intestinal epithelia. These data indicate that non-cell-autonomous metabolic modulation is a crucial regulator for cell competition, shedding light on the unexplored events at the initial stage of carcinogenesis.

INTRODUCTION

It remains enigmatic what happens at the initial stage of carcinogenesis where oncogenic transformation occurs in a single cell within the epithelium[1-3]. Recent studies have demonstrated that newly emerging transformed cells are often eliminated from epithelial tissues via cell competition against the neighbouring normal epithelial cells. Cell competition is a process by which two different cell populations, upon interaction, compete with each other for survival and space; consequently, the loser cells are eliminated from the tissues, while the winner cells occupy the vacant spaces. This phenomenon was originally found and has been extensively studied in *Drosophila*[4-9]. But, recent studies have revealed that cell competition can also occur in mammals between normal and various types of transformed epithelial cells. For example, RasV12-, Src- or erbB2-transformed cells are apically extruded when they are surrounded by normal epithelial cells[10-13]. In addition, tumour suppressor protein Scribble- or Mahjong-knockdown cells undergo apoptosis and leave a monolayer of normal epithelial cells[7, 14]. Importantly, when transformed cells alone are present, neither apical extrusion nor apoptosis occurs, indicating that the presence of the surrounding normal cells profoundly influences the behaviour and fate of transformed cells.

We and other groups have explored the molecular mechanisms of cell competition between normal and RasV12-transformed epithelial cells and revealed that various non-cell-autonomous changes occur in both cells at their interface. For instance, normal epithelial cells accumulate cytoskeletal protein Filamin at the interface with the adjacent transformed cells, thereby actively eliminating them[15]. This implies a notion that normal epithelial cells have anti-tumour activity that does not involve

immune cells: a process termed EDAC (Epithelial Defence Against Cancer)[15]. By contrast, in RasV12-transformed cells that are surrounded by normal cells, actin-binding protein Epithelial Protein Lost In Neoplasm (EPLIN) is accumulated[16]. The accumulated EPLIN then activates the downstream molecules such as PKA and myosin-II, which positively regulate apical extrusion of RasV12 cells. However, the molecular mechanisms of how EDAC from normal cells affects the neighbouring transformed cells and promotes their elimination are still poorly understood.

Cellular metabolism is dynamically modulated and adjusted in accordance with various conditions. For example, at the later stage of cancer development, aerobic glycolysis is enhanced in tumour cells, often accompanied by the downregulation of mitochondrial activity; these metabolic changes are called Warburg effect[17-21]. But, it is not clearly understood whether cellular metabolism is also affected at the initial stage of carcinogenesis. In this study, we have examined whether and how the metabolic status is regulated at the interface between normal and newly emerging transformed epithelial cells.

RESULTS

Warburg effect-like metabolic changes occur in RasV12-transformed cells that are surrounded by normal cells

To examine the involvement of metabolic regulation in cell competition, we first examined mitochondrial energy metabolism at the interface between normal and RasV12-transformed epithelial cells. TMRM (tetramethylrhodamine methyl ester) is a positively charged red fluorescent dye that accumulates in active mitochondria according to the negative membrane potential gradient across their inner membranes. We found that the TMRM fluorescence, but not the fluorescence of a control dye CMTPX, was strongly reduced in RasV12-transformed epithelial cells surrounded by normal epithelial cells compared to that in RasV12-transformed cells cultured alone or in GFP-expressing cells surrounded by normal cells (Fig. 1a-c, g). The comparable phenomenon was also observed in Src-transformed cells, but not in Scribble-knockdown cells (Supplementary Fig. 1a, b). The decreased incorporation of TMRM was observed in both apically extruding and extruded RasV12 cells (Fig. 1d). The non-cell-autonomous downregulation of mitochondrial membrane potential was also confirmed by using mitoSOX, an indicator for mitochondrial superoxide production that reflects mitochondrial ATP production (Fig. 1e-g). Immunofluorescence of the mitochondrial resident protein Tom20 or MitoTracker Green fluorescence which is incorporated into mitochondria in a membrane potential-independent manner showed that the number of mitochondria was not altered in RasV12 cells surrounded by normal cells (Fig. 1h and Supplementary Fig. 1c-h). In addition, by electron microscopic analyses, mitophagosome-like structures were frequently observed in RasV12 cells that were surrounded by normal epithelial cells (Supplementary Fig. 2). Collectively, these data imply that the decreased TMRM incorporation does not result

from a change in mitochondrial mass, but from a change in mitochondrial function. Furthermore, we found that incorporation of glucose analogue 2-NBDG was enhanced in RasV12 cells surrounded by normal cells (Fig. 2a, b), suggesting that uptake of glucose is enhanced in a non-cell-autonomous fashion. Moreover, expression of LDHA, which converts pyruvate to lactate, was significantly increased in RasV12-transformed cells that were surrounded by normal cells (Fig. 2c-e and Supplementary Fig. 3a). Accordingly, lactate secretion was higher in RasV12 cells than normal cells, and was further enhanced when RasV12 cells were surrounded by normal cells (Fig. 2f). This non-cell-autonomous increase in lactate secretion was abolished when LDHA was knocked down in RasV12 cells (Fig. 2f and Supplementary Fig. 4e). These data indicate that the interaction with the neighbouring normal epithelial cells potentiates the Warburg effect-like metabolic changes in transformed cells: downregulation of mitochondrial function and enhanced aerobic glycolysis.

PDK4 plays a crucial role in the decreased mitochondrial membrane potential and apical extrusion of RasV12-transformed cells surrounded by normal cells

To reveal the molecular mechanism that causes the Warburg effect-like phenomenon, we examined expression of various metabolic enzymes by quantitative real-time PCR and found that expression of pyruvate dehydrogenase kinase 4 (PDK4) was significantly elevated in RasV12-transformed cells when they were co-cultured with normal cells (Fig. 3a). PDK4 phosphorylates and thus inactivates pyruvate dehydrogenase (PDH) that catalyses conversion of pyruvate to acetyl-CoA, thereby blocking the entry into the TCA cycle (Supplementary Fig. 3a). Indeed, phosphorylation of PDH was also enhanced in RasV12 cells when they were

surrounded by normal cells (Fig. 3b-d). To examine the functional involvement of PDK4, we established RasV12-transformed cells stably expressing PDK4-shRNA (Fig. 3e) and CRISPR-edited PDK4-knockout RasV12-transformed cells (Supplementary Fig. 3b). PDK4-knockdown or PDK4-knockout suppressed PDH phosphorylation and significantly restored TMRM incorporation in RasV12 cells surrounded by normal cells (Fig. 3f, g and Supplementary Fig. 3c-g), suggesting that upregulation of PDK4 is, at least partly, responsible for the decreased mitochondrial membrane potential. PDK4-knockdown or -knockout also suppressed LDHA accumulation (Supplementary Fig. 3h-j). Interestingly, PDK4-knockdown or -knockout drastically suppressed apical extrusion of RasV12 cells, while promoting formation of basal protrusions that extended beneath the neighbouring normal cells (Fig. 3h, i and Supplementary Fig. 3k-n). DCA is a specific inhibitor of the PDK family[22, 23] of which upregulation is often observed in the later stage of cancer[24-27]. Therefore, DCA has been intensively tested in clinical trials for treatment of malignant cancer including glioblastoma and various solid tumours[28-31]. We found that treatment of DCA caused the comparable effect to that induced by PDK4 knockdown/knockout: suppression of PDH phosphorylation (Fig. 4a), restoration of TMRM incorporation (Fig. 4b, c) and suppression of apical extrusion and promotion of basal protrusions (Fig. 4d, e). We also demonstrated that another PDK inhibitor Radicicol phenocopied the effect of DCA (Supplementary Fig. 4a-d). DCA treatment also suppressed elevated LDHA expression in RasV12 cells surrounded by normal cells (Fig. 4a). In contrast, knockdown of LDHA in RasV12 cells did not affect TMRM incorporation (Supplementary Fig. 4e, f), suggesting that decreased mitochondrial membrane potential causes LDHA upregulation. Moreover, knockdown of LDHA moderately suppressed apical extrusion (Supplementary Fig.

4g). These results imply that the PDK4-mediated Warburg effect-like metabolic alteration influences the behaviour of transformed cells and promotes their elimination from epithelia. When PDH-knockdown cells were surrounded by normal cells, apical extrusion did not occur (Supplementary Fig. 4h-j), indicating that downregulation of mitochondrial membrane potential alone is not sufficient to cause apical extrusion. Thus, while the non-cell-autonomously induced metabolic changes play an indispensable role in the elimination of transformed cells, additional, unidentified molecular mechanisms are also involved in this process, which need to be explored in future studies.

EDAC and EPLIN act upstream of the Warburg effect-like metabolic changes in RasV12 cells surrounded by normal cells

We further examined the molecular mechanism underlying the Warburg effect-like phenomenon. In a previous study, we demonstrated that EPLIN accumulates in RasV12-transformed cells surrounded by normal cells and plays a positive role in the apical extrusion via activation of the downstream molecules, protein kinase A (PKA) and myosin-II[16]. We found that knockdown of EPLIN in RasV12 cells significantly restored mitochondrial membrane potential (Fig. 5a, b and Supplementary Fig. 5a). In addition, EPLIN-knockdown suppressed PDK4 upregulation, phosphorylation of PDH and LDHA accumulation (Fig. 5c, d and Supplementary Fig. 5b). These data indicate that EPLIN is a crucial upstream regulator of the Warburg effect-like metabolic changes. Furthermore, we examined the effect of various inhibitors on TMRM incorporation and apical extrusion. Concerning downstream molecules of EPLIN, PKA inhibitor KT5720 reverted TMRM incorporation, whereas myosin-II inhibitor Blebbistatin did not (Supplementary Fig. 5c and Supplementary Fig. 8a).

The other tested inhibitors (Cytochalasin D, NAC, 3-MA, Y27632, L-NAME) did not affect TMRM incorporation (Supplementary Fig. 5c and Supplementary Fig. 8a), indicating the specific effect of KT5720 on TMRM incorporation. Furthermore, KT5720 did not significantly affect expression of PDK4. These data suggest that EPLIN regulates those metabolic changes via PDK4- and PKA-dependent pathways (Supplementary Fig. 8c).

It was previously reported that normal epithelial cells can recognize and actively eliminate the neighbouring transformed cells, in which Filamin in the normal cells plays an important role, at least partly, by inducing the accumulation of EPLIN in transformed cells[15, 16]; this tumour-suppressing process is called EDAC[15]. When RasV12 cells were surrounded by EDAC-deficient Filamin-knockdown cells, TMRM incorporation in RasV12 cells was restored, instead rather promoted in comparison to that in the surrounding knockdown cells (Fig. 5e, f and Supplementary Fig. 3f and 5a). In addition, knockdown of Filamin in the surrounding normal cells substantially suppressed phosphorylation of PDH and accumulation of LDHA (Fig. 5g and Supplementary Fig. 3d, i and 5b). Collectively, these data demonstrate that EDAC from normal cells induces the metabolic alterations of the neighbouring transformed cells via EPLIN, thereby promoting elimination of the transformed cells from epithelia (Supplementary Fig. 8c).

Upregulation of the glycolytic pathway plays a positive role in the elimination of RasV12-transformed cells

What is the functional significance of EDAC-induced Warburg effect-like metabolic changes in the apical elimination of transformed cells? The metabolic shift from mitochondrial oxidative phosphorylation to glycolysis can affect various cellular

processes such as glucose metabolism, ATP production and resistance to ROS-mediated oxidative stress. Using a glucose-FRET probe, we found that intracellular glucose concentration was substantially diminished in RasV12 cells surrounded by normal cells (Fig. 6a-c), indicating that intracellular glucose is exhausted via massively elevated glycolysis despite of the increased glucose uptake (Fig. 2a, b). The comparable glucose metabolic condition is also reported in conventional Warburg effect[32-34]. In addition, the result with the FRET-based ATP sensor (ATeam) showed that the ATP level was moderately increased in RasV12-transformed cells that were surrounded by normal cells (Supplementary Fig. 5d-f), suggesting that the ATP production is fully compensated and even promoted by the enhanced glycolytic pathway. To further understand the functional significance of this process, we examined the effect of a hexokinase inhibitor 2-deoxy-D-glucose (2-DG). Addition of 2-DG diminished the non-cell-autonomously upregulated ATP level (Supplementary Fig. 5e-g) and significantly suppressed apical extrusion of RasV12 cells surrounded by normal cells (Supplementary Fig. 5h, i), indicating that the upregulation of the glycolytic pathway plays a positive role in the elimination of transformed cells. The ATP production speed via glycolysis is far greater than that via mitochondria[35], hence the metabolic shift to glycolysis may be of benefit to transformed cells by supporting prompt energy supply required for the dynamic process of apical extrusion.

PDK-mediated mitochondrial dysfunction induces apical elimination of RasV12-transformed cells *ex vivo* and *in vivo*

To understand the generality and functional significance of these findings, we established an LSL-RasV12-IRES-eGFP mouse whereby RasV12 expression is induced in a Cre-dependent fashion and traced by simultaneous expression of eGFP

(Supplementary Fig. 6a, b). By crossing a Villin-Cre-ERT2 mouse with an LSL-RasV12-IRES-eGFP mouse, we obtained a novel cell competition mouse model (Fig. 7a). Administration of a low dose of tamoxifen induces recombination events less frequently, resulting in expression of RasV12 in a mosaic manner within intestinal epithelia (Supplementary Fig. 6c). Using this system, we examined the fate of newly emerging RasV12-transformed cells that are surrounded by normal epithelial cells *ex vivo* and *in vivo*. First, intestinal epithelial cells were collected from these mice and were subjected to crypt organoid culture in the matrigel, followed by tamoxifen treatment[36]. At 12-24 h after treatment with a low dose of tamoxifen, RasV12-expressing cells were apically shifted with wedge-like morphology; at 36-48 h, RasV12 cells were detached from the basement membrane and eventually extruded into the apical lumen (Fig. 7b, top). In contrast, cells expressing only GFP remained within the epithelium, and apical extrusion did not frequently occur (Fig. 7b, bottom). When RasV12 were predominantly expressed in the whole epithelium by a high dose of tamoxifen, the frequency of apical extrusion was strongly suppressed (Fig. 7c), indicating that the presence of the surrounding normal cells induced the elimination of transformed cells in the *ex vivo* system as well. We also found that EPLIN was accumulated in RasV12 cells surrounded by normal cells in a non-cell-autonomous fashion (Supplementary Fig. 7a). Time-lapse analyses of the crypt organoid culture revealed that the event of apical extrusion took rather variable times between 2-20 h and that the extruded transformed cells disappeared into the apical lumen (Supplementary Fig. 7b and Supplementary Movie 1-3). Thus, we have successfully established a brand-new mouse model system, in which apical elimination of RasV12-transformed cells can be captured three-dimensionally. Using this experimental system, we found that TMRM incorporation was diminished in both extruding and

extruded RasV12-expressing cells that were surrounded by normal cells (Fig. 7d, first and second upper panels, e), but not in RasV12-expressing cells surrounded by themselves or in GFP-expressing cells (Fig. 7d, third and fourth panels, e). In addition, phosphorylation of PDH was elevated in RasV12 cells surrounded by normal cells (Fig. 7f). Furthermore, DCA treatment restored the TMRM incorporation and suppressed the apical extrusion of RasV12 cells (Fig. 7g, h and Supplementary Fig. 7c, d). Finally, we examined the fate of RasV12-transformed cells *in vivo*. Intraperitoneal injection of a low dose of tamoxifen induced RasV12 expression in a mosaic manner within the intestinal epithelium, and most of RasV12-expressing cells were apically eliminated after three days of tamoxifen treatment, whereas GFP-expressing cells remained in the epithelial layer (Fig. 8a-c). Using two-photon microscopic *in vivo* time-lapse imaging, the dynamic mode of apical extrusion of RasV12-expressing cells was captured (Fig. 8d and Supplementary Movie 4). Finally, we examined the functional role of PDK in the elimination of RasV12 cells from epithelia *in vivo*. When DCA was administered, apical extrusion of RasV12 cells was significantly suppressed (Fig. 8e, f). Furthermore, we used the recently established iGT (intestine-specific gene transfer) system where mouse intestinal epithelia can be transfected with siRNA using HVJ-E (haemagglutinating virus of Japan envelope) (Fig. 8g, h)[37]. We then demonstrated that knockdown of PDK4 significantly suppressed apical extrusion (Fig. 8i-k). Collectively, these data suggest that apical elimination of RasV12-transformed cells occurs *ex vivo* and *in vivo*, which is promoted by the PDK4-mediated mitochondrial downregulation.

Discussion

The glycolytic pathway and mitochondrial function are frequently de-regulated in neoplastic cells in various ways. These metabolic alterations are generally thought to promote cancer progression, though its biological and pathological significance still remains elusive[17-20]. Indeed, clinical trials targeting derailed mitochondrial metabolism, such as with DCA, are currently undergoing[28-31]. By contrast, our study suggests that the Warburg effect-like metabolic changes can occur at the early stage of carcinogenesis in a non-cell-autonomous fashion and that DCA treatment could potentially suppress eradication of newly emerging transformed cells. Thus, the adverse effect of DCA may need to be carefully re-examined for the longer time periods.

The EDAC-mediated Warburg effect-like metabolic shift does not accommodate several features of the prevailing Warburg effect (Supplementary Fig. 8b). Conventional Warburg effect, which is often observed at the relatively late phase of cancer progression, is caused by various genetic and epigenetic insults and adaptation to harsh tumour microenvironments. In contrast, EDAC-induced Warburg effect-like metabolic changes are triggered by the inputs from neighbouring normal cells at the initial stage of carcinogenesis. The conventional Warburg effect is generally associated with upregulation of HIF1, PDK1/3 and PKM2[38-45], whereas in EDAC-induced Warburg effect-like metabolic changes the expression of these enzymes is not elevated, instead EPLIN and PDK4 act as key upstream regulators. Moreover, the most crucial difference between conventional Warburg effect and EDAC-induced metabolic changes is their roles in tumourigenesis; the former generally plays a tumour-promoting role, whereas the latter potentially plays a tumour-suppressive role by actively eliminating transformed cells. Thus, though these two processes share

similar metabolic alterations (mitochondrial downregulation and increased aerobic glycolysis), they are governed by distinct upstream and downstream mediators.

HIF1 is a crucial regulator for Warburg effect by modulating multiple metabolic pathways including the TCA cycle and glycolytic pathway[46]. Therefore, we explored the involvement of HIF1 in EDAC-induced Warburg effect-like metabolic changes. By using the 5xHRE (HIF1 responsive element) reporter assay, we found that HIF1 activity was not enhanced in RasV12 cells surrounded by normal cells, compared with that in RasV12 cells cultured alone (Supplementary Fig. 7e). It has been reported that HIF1 enhances transcription of PDK1/3 and LDHA, thereby inducing Warburg effect[46]. But, qRT-PCR analysis demonstrated that the mRNA level of PDK1/3 or LDHA was not increased in RasV12 cells surrounded by normal cells (Fig. 3a). Thus, we could not obtain evidence showing the involvement of HIF1 in EDAC-induced metabolic changes, and our data suggest that LDHA is post-transcriptionally upregulated by a HIF1-independent, unknown mechanism.

In this study, we have mainly used fluorescence imaging to demonstrate the non-cell-autonomous changes between normal and transformed epithelial cells. In the research field of cell competition, the researchers have struggled with the technical problem: biochemical analyses of each cell population in co-cultures. The non-cell-autonomous changes induced by the neighbouring normal cells are regulated temporally and dynamically, thus once the interaction with normal cells is disrupted, the non-cell-autonomous biochemical changes (not the mRNA level) will instantly vanish. To perform biochemical analyses for each cell population, the co-cultured epithelial cells should be first treated with trypsin to disrupt cell-cell adhesions and dissociate cells from each other, which will be then FACS sorted for a few hours. Despite of the substantial number of trials, we have found just minor remaining non-

cell-autonomous traces after those procedures. To further intensify the findings in this study, we need to exploit new methods such as FRET probes for metabolites in future studies.

A previous study in *Drosophila* has shown that mitochondrial metabolism can be regulated during cell competition[47]. Our data in this study demonstrate that metabolic modulation is a crucial regulator for cell competition between normal and transformed epithelial cells in mammals as well. Further elucidation of the molecular mechanisms that drive the EDAC-induced metabolic changes will lead to novel approaches for cancer prevention.

References

1. Hanahan, D. & Weinberg, R.A. Hallmarks of cancer: the next generation. *Cell* **144**, 646-674 (2011).
2. Fialkow, P.J. Clonal origin of human tumors. *Biochimica et biophysica acta* **458**, 283-321 (1976).
3. Nowell, P.C. The clonal evolution of tumor cell populations. *Science* **194**, 23-28 (1976).
4. Morata, G. & Ripoll, P. Minutes: mutants of drosophila autonomously affecting cell division rate. *Dev Biol* **42**, 211-221 (1975).
5. de la Cova, C., Abril, M., Bellosta, P., Gallant, P. & Johnston, L.A. Drosophila myc regulates organ size by inducing cell competition. *Cell* **117**, 107-116 (2004).
6. Moreno, E. & Basler, K. dMyc transforms cells into super-competitors. *Cell* **117**, 117-129 (2004).
7. Tamori, Y. *et al.* Involvement of Lgl and Mahjong/VprBP in cell competition. *PLoS Biol* **8**, e1000422 (2010).
8. Karim, F.D. & Rubin, G.M. Ectopic expression of activated Ras1 induces hyperplastic growth and increased cell death in Drosophila imaginal tissues. *Development* **125**, 1-9 (1998).
9. Brumby, A.M. & Richardson, H.E. scribble mutants cooperate with oncogenic Ras or Notch to cause neoplastic overgrowth in Drosophila. *The EMBO journal* **22**, 5769-5779 (2003).
10. Hogan, C. *et al.* Characterization of the interface between normal and transformed epithelial cells. *Nat Cell Biol* **11**, 460-467 (2009).
11. Kajita, M. *et al.* Interaction with surrounding normal epithelial cells influences signalling pathways and behaviour of Src-transformed cells. *J Cell Sci* **123**, 171-180 (2010).
12. Wu, S.K. *et al.* Cortical F-actin stabilization generates apical-lateral patterns of junctional contractility that integrate cells into epithelia. *Nat Cell Biol* **16**, 167-178 (2014).
13. Leung, C.T. & Brugge, J.S. Outgrowth of single oncogene-expressing cells from suppressive epithelial environments. *Nature* **482**, 410-413 (2012).
14. Norman, M. *et al.* Loss of Scribble causes cell competition in mammalian cells. *J Cell Sci* **125**, 59-66 (2012).
15. Kajita, M. *et al.* Filamin acts as a key regulator in epithelial defence against transformed cells. *Nature communications* **5**, 4428 (2014).
16. Ohoka, A. *et al.* EPLIN is a crucial regulator for extrusion of RasV12-transformed cells. *J Cell Sci* **128**, 781-789 (2015).
17. Vander Heiden, M.G., Cantley, L.C. & Thompson, C.B. Understanding the Warburg effect: the metabolic requirements of cell proliferation. *Science* **324**, 1029-1033 (2009).
18. Sciacovelli, M., Gaude, E., Hilvo, M. & Frezza, C. The metabolic alterations of cancer cells. *Methods in enzymology* **542**, 1-23 (2014).
19. Koppenol, W.H., Bounds, P.L. & Dang, C.V. Otto Warburg's contributions to current concepts of cancer metabolism. *Nat Rev Cancer* **11**, 325-337 (2011).
20. Cairns, R.A., Harris, I.S. & Mak, T.W. Regulation of cancer cell metabolism. *Nat Rev Cancer* **11**, 85-95 (2011).
21. Warburg, O. On the origin of cancer cells. *Science* **123**, 309-314 (1956).

22. Kato, M., Li, J., Chuang, J.L. & Chuang, D.T. Distinct structural mechanisms for inhibition of pyruvate dehydrogenase kinase isoforms by AZD7545, dichloroacetate, and radicicol. *Structure* **15**, 992-1004 (2007).
23. Wynn, R.M. *et al.* Pyruvate dehydrogenase kinase-4 structures reveal a metastable open conformation fostering robust core-free basal activity. *The Journal of biological chemistry* **283**, 25305-25315 (2008).
24. Sutendra, G. *et al.* Mitochondrial activation by inhibition of PDKII suppresses HIF1a signaling and angiogenesis in cancer. *Oncogene* **32**, 1638-1650 (2013).
25. Koukourakis, M.I. *et al.* Pyruvate dehydrogenase and pyruvate dehydrogenase kinase expression in non small cell lung cancer and tumor-associated stroma. *Neoplasia* **7**, 1-6 (2005).
26. Hur, H. *et al.* Expression of pyruvate dehydrogenase kinase-1 in gastric cancer as a potential therapeutic target. *International journal of oncology* **42**, 44-54 (2013).
27. Lu, C.W. *et al.* Overexpression of pyruvate dehydrogenase kinase 3 increases drug resistance and early recurrence in colon cancer. *The American journal of pathology* **179**, 1405-1414 (2011).
28. Chu, Q.S. *et al.* A phase I open-labeled, single-arm, dose-escalation, study of dichloroacetate (DCA) in patients with advanced solid tumors. *Investigational new drugs* **33**, 603-610 (2015).
29. Dunbar, E.M. *et al.* Phase 1 trial of dichloroacetate (DCA) in adults with recurrent malignant brain tumors. *Investigational new drugs* **32**, 452-464 (2014).
30. Strum, S.B. *et al.* Case report: Sodium dichloroacetate (DCA) inhibition of the "Warburg Effect" in a human cancer patient: complete response in non-Hodgkin's lymphoma after disease progression with rituximab-CHOP. *Journal of bioenergetics and biomembranes* **45**, 307-315 (2013).
31. Garon, E.B. *et al.* Dichloroacetate should be considered with platinum-based chemotherapy in hypoxic tumors rather than as a single agent in advanced non-small cell lung cancer. *Journal of cancer research and clinical oncology* **140**, 443-452 (2014).
32. Kami, K. *et al.* Metabolomic profiling of lung and prostate tumor tissues by capillary electrophoresis time-of-flight mass spectrometry. *Metabolomics : Official journal of the Metabolomic Society* **9**, 444-453 (2013).
33. Shestov, A.A. *et al.* Quantitative determinants of aerobic glycolysis identify flux through the enzyme GAPDH as a limiting step. *eLife* **3** (2014).
34. Tang, X. *et al.* A joint analysis of metabolomics and genetics of breast cancer. *Breast cancer research : BCR* **16**, 415 (2014).
35. Pfeiffer, T., Schuster, S. & Bonhoeffer, S. Cooperation and competition in the evolution of ATP-producing pathways. *Science* **292**, 504-507 (2001).
36. Sato, T. *et al.* Single Lgr5 stem cells build crypt-villus structures in vitro without a mesenchymal niche. *Nature* **459**, 262-265 (2009).
37. Imajo, M., Ebisuya, M. & Nishida, E. Dual role of YAP and TAZ in renewal of the intestinal epithelium. *Nat Cell Biol* **17**, 7-19 (2015).
38. Semenza, G.L., Roth, P.H., Fang, H.M. & Wang, G.L. Transcriptional regulation of genes encoding glycolytic enzymes by hypoxia-inducible factor 1. *The Journal of biological chemistry* **269**, 23757-23763 (1994).
39. Gordan, J.D., Thompson, C.B. & Simon, M.C. HIF and c-Myc: sibling rivals for control of cancer cell metabolism and proliferation. *Cancer Cell* **12**, 108-113 (2007).

40. Kim, J.W., Tchernyshyov, I., Semenza, G.L. & Dang, C.V. HIF-1-mediated expression of pyruvate dehydrogenase kinase: a metabolic switch required for cellular adaptation to hypoxia. *Cell metabolism* **3**, 177-185 (2006).
41. Papandreou, I., Cairns, R.A., Fontana, L., Lim, A.L. & Denko, N.C. HIF-1 mediates adaptation to hypoxia by actively downregulating mitochondrial oxygen consumption. *Cell metabolism* **3**, 187-197 (2006).
42. Kluza, J. *et al.* Inactivation of the HIF-1alpha/PDK3 signaling axis drives melanoma toward mitochondrial oxidative metabolism and potentiates the therapeutic activity of pro-oxidants. *Cancer research* **72**, 5035-5047 (2012).
43. Atsumi, T. *et al.* High expression of inducible 6-phosphofructo-2-kinase/fructose-2,6-bisphosphatase (iPFK-2; PFKFB3) in human cancers. *Cancer research* **62**, 5881-5887 (2002).
44. Christofk, H.R. *et al.* The M2 splice isoform of pyruvate kinase is important for cancer metabolism and tumour growth. *Nature* **452**, 230-233 (2008).
45. Wu, W. & Zhao, S. Metabolic changes in cancer: beyond the Warburg effect. *Acta biochimica et biophysica Sinica* **45**, 18-26 (2013).
46. Semenza, G.L. HIF-1: upstream and downstream of cancer metabolism. *Current opinion in genetics & development* **20**, 51-56 (2010).
47. de la Cova, C. *et al.* Supercompetitor status of Drosophila Myc cells requires p53 as a fitness sensor to reprogram metabolism and promote viability. *Cell metabolism* **19**, 470-483 (2014).
48. Levayer, R., Hauert, B. & Moreno, E. Cell mixing induced by myc is required for competitive tissue invasion and destruction. *Nature* **524**, 476-480 (2015).

ACKNOWLEDGEMENTS

We thank K. Rajewsky for the establishment of knocked-in ES cells harbouring RasV12-eGFP. We also thank H. Harada for the HIF1 reporter-expressing vector, C. Kuo for the R-spondin-producing cell line and T. Yoshimori for useful advice on EM analyses. Ya.F. is supported by Japan Society for the Promotion of Science (JSPS) Grant-in-Aid for Scientific Research on Innovative Areas 26114001, Grant-in-Aid for Scientific Research (A) 26250026 and AMED Strategic Japanese-Swiss Cooperative Program. Ya.F. is also supported by the Takeda Science Foundation. Shu.K. is supported by Japan Society for the Promotion of Science (JSPS) Grant-in-Aid for Scientific Research on Innovative Areas 26112701, Kato Memorial Bioscience Foundation and The YASUDA Medical Foundation.

AUTHOR CONTRIBUTIONS

Shu.K. designed experiments and generated most of the data. K.I. performed qRT-PCR experiments and metabolic analyses. H.K. and Sho.K. designed and analysed the cell competition mouse model. S.I., H.Y., Y.Y., To.Ma., H.W., Ri.E., A.N., I.K., S.T., R.N. and Ta. M. assisted experiments. M.K., A.S., Ry.E., S.H., S.Y., J.K. and M.Is. performed time-lapse experiments. T.K. performed electron microscopic analyses. J.M.N., Ya.O., Yo.F. and Yu.O. performed FRET analysis. H.I., To.So. and M.R.D. assisted metabolic analyses. Y. S., M.O., J.M. and T.Sa. assisted *ex vivo* and *in vivo* experiments. Ta.S., To.Mo., M.Im. and E.N. assisted iGT experiments. Ya.F. conceived and designed the study. The manuscript was written by Shu.K. and Ya.F. with assistance from the other authors.

COMPETING FINANCIAL INTERESTS

The authors declare no competing financial interests.

Figure legends

Figure 1. Mitochondrial membrane potential is diminished in RasV12-transformed cells that are surrounded by normal epithelial cells. (**a**-**g**) Incorporation of TMRM or mitoSOX in RasV12-transformed cells surrounded by normal cells. (**a**, **d**, **e**) Confocal images of MDCK-pTR GFP-RasV12 or MDCK-pTR GFP cells mixed with normal MDCK cells, or cultured alone. Cells were loaded with 50 nM TMRM (red) (**a**, **b**, **d**) or 5 μM MitoSOX (red) (**e**, **f**). Arrows indicate RasV12-transformed cells showing diminished TMRM (**a**) or mitoSOX (**e**) fluorescence. (**b**, **f**) Quantification of the fluorescence intensity of TMRM (**b**) or mitoSOX (**f**). Data are mean ± s.e.m.. Values are expressed as a ratio relative to MDCK. **P*<0.001, unpaired two-tailed t-test; n=92, 24, 53 and 60 cells (**b**) or n=52, 45 and 31 cells (**f**) pooled from three independent experiments. (**c**) CMTPX incorporation in RasV12-transformed cells. MDCK-pTR GFP-RasV12 cells were mixed with normal MDCK cells or cultured alone, and loaded with 5 μM CMTPX (red). (**d**) Confocal images of xz sections of apically extruding or extruded RasV12-transformed cells surrounded by normal cells and of RasV12-transformed cells cultured alone. (**g**) The measurement of fluorescence intensity of TMRM or MitoSOX using image cytometer in MDCK-pTR GFP-RasV12 cells mixed with normal MDCK cells or cultured alone. Cells were loaded with 50 nM TMRM or 5 μM MitoSOX.(**h**) Immunofluorescence images of Tom20. MDCK-pTR GFP-RasV12 cells were mixed with normal MDCK cells or cultured alone, and were stained with Hoechst 33342 (blue) and anti-Tom20 antibody (red). Scale bars, 10 μm (**a**, **c**-**e**, **h**). Statistics source data for **b**, **f** are provided in Supplementary Table 2.

Figure 2. Warburg effect-like metabolic changes in RasV12-transformed cells that are surrounded by normal cells. (**a**) 2-NBDG incorporation in myc-RasV12 cells. MDCK-pTRE3G myc-RasV12 cells co-cultured with MDCK cells or cultured alone were loaded with 100 μM 2-NBDG. (**b**) Quantification of the fluorescence intensity of 2-NBDG. Data are mean ± s.e.m.. Values are expressed as a ratio relative to MDCK. **P*<0.001, unpaired two-tailed t-test; n=66, 66 and 48 cells pooled from three independent experiments. (**c**) Accumulation of LDHA in RasV12-transformed cells surrounded by normal cells. MDCK-pTR GFP-RasV12 cells were mixed with normal MDCK cells or cultured alone, and were stained with Hoechst 33342 (blue), anti-LDHA antibody (red) and Alexa-Fluor-647-conjugated phalloidin (white). Scale bars, 10 μm (**a**, **c**). (**d**) Quantification of the percentage of LDHA-enriched RasV12-transformed cells. Data are mean ± s.e.m.. **P*<0.05, unpaired two-tailed t-test; n= two independent experiments, each having 279 and 233 cells quantified. (**e**) The measurement of fluorescence intensity of LDHA using image cytometer in MDCK-pTR GFP-RasV12 cells mixed with normal MDCK cells or cultured alone. Cells were stained with Hoechst 33342 and anti-LDHA antibody. (**f**) Lactate concentration in the conditioned medium at 12-24 h after tetracycline addition. The mean values of the indicated single cultures are also shown as the gray bars. Data are mean ± s.e.m.. **P*<0.001, unpaired two-tailed t-test; n= five independent experiments for MDCK alone, RasV12 alone and MDCK:RasV12=1:1, two independent experiments for RasV12 shLDHA1 alone and MDCK:RasV12 shLDHA1=1:1 and three independent experiments for RasV12 shLDHA2 alone and MDCK:RasV12 shLDHA2=1:1. Statistics source data for **b**, **d**, **f** are provided in Supplementary Table 2.

Figure 3. PDK4 plays a crucial role in the decreased mitochondrial membrane potential and apical extrusion of RasV12-transformed cells surrounded by normal cells. (**a**) Quantitative RT-PCR analysis of various metabolic enzymes in RasV12-transformed cells surrounded by normal cells. MDCK-pTR GFP-RasV12 cells were co-cultured with normal MDCK cells or cultured alone. GFP-positive RasV12 cells were selectively collected by FACS sorting and subjected to qPCR analysis. Values are shown as fold change in RasV12 cells surrounded by normal cells relative to RasV12 cells cultured alone. Data are mean ± s.e.m.. **P*<0.05, unpaired two-tailed t-test; n= three or four independent experiments. (**b**) Immunofluorescence images of phosphorylated PDH. MDCK-pTR GFP-RasV12 were mixed with normal MDCK cells or cultured alone, and were stained with Hoechst 33342 (blue) and anti-p-PDH antibody (red). (**c**) Quantification of the fluorescence intensity of p-PDH. Data are mean ± s.e.m.. Values are expressed as a ratio relative to MDCK. **P*<0.005, unpaired two-tailed t-test; n=93, 147 and 89 cells pooled from three independent experiments. (**d**) The measurement of fluorescence intensity of p-PDH using image cytometer in MDCK-pTR GFP-RasV12 cells mixed with normal MDCK cells or cultured alone. Cells were stained with Hoechst 33342 and anti-p-PDH antibody. (**e**-**i**) Effect of PDK4-knockdown on TMRM incorporation (**f**, **g**) or apical extrusion (**h**, **i**) of RasV12 cells surrounded by normal cells. (**e**) Establishment of MDCK-pTR GFP-RasV12 cells stably expressing PDK4-shRNA1 or -shRNA2. Knockdown of PDK4 was confirmed by quantitative RT-PCR. Data are mean ± s.e.m.. **P*<0.01, unpaired two-tailed t-test; n= three independent experiments. (**f**) MDCK-pTR GFP-RasV12 PDK4-shRNA1 or -shRNA2 cells were mixed with normal MDCK cells and loaded with TMRM. (**g**) Quantification of the fluorescence intensity of TMRM. Data are mean ± s.e.m.. Values are expressed as a ratio relative to MDCK. **P*<0.001, unpaired

two-tailed t-test; n= 92, 92, 97 and 102 cells pooled from three independent experiments. (**h**) Immunofluorescence images of xz sections of MDCK-pTR GFP-RasV12 PDK4-shRNA1 or -shRNA2 cells surrounded by normal MDCK cells. Arrowheads indicate the basal protrusion. Scale bars, 10 μm (**b**, **f**, **h**). (**i**) Quantification of the apical extrusion and basal protrusion formation. Data are mean ± s.e.m.. **P*<0.05, unpaired two-tailed t-test; n=three independent experiments, each having 311 and 312 cells quantified. Statistics source data for **a**, **c**, **e**, **g**, **i** are provided in Supplementary Table 2.

Figure 4. DCA treatment abolishes the Warburg effect-like metabolic changes and suppresses apical extrusion of RasV12-transformed cells. (**a**) Effect of DCA on p-PDH or LDHA. MDCK-pTR GFP-RasV12 cells were mixed with normal MDCK cells in the absence or presence of 25 mM DCA. Cells were stained with Hoechst 33342 (blue) and anti-p-PDH or anti-LDHA antibody (red). (**b**-**e**) Effect of DCA on TMRM incorporation (**b**, **c**) or apical extrusion (**d**, **e**) of RasV12-transformed cells. (**b**) MDCK-pTR GFP-RasV12 cells were co-cultured with normal MDCK cells in the absence or presence of 25 mM DCA and incubated with 50 nM TMRM. (**c**) Quantification of the fluorescence intensity of TMRM. Data are mean ± s.e.m.. Values are expressed as a ratio relative to MDCK (-DCA). **P*<0.001, unpaired two-tailed t-test; n= 84, 82, 98 and 90 cells pooled from three independent experiments. (**d**) Immunofluorescence images of xz sections of MDCK-pTR GFP-RasV12 cells surrounded by normal MDCK cells in the absence or presence of DCA. An arrowhead indicates the basal protrusion. Scale bars, 10 μm (**a**, **b**, **d**). (**e**) Quantification of the apical extrusion and basal protrusion formation of RasV12 cells in the absence or presence of DCA. Data are mean ± s.e.m.. **P*<0.05, unpaired two-tailed t-test;

n=three independent experiments, each having 418 and 432 cells quantified. Statistics source data for **c**, **e** are provided in Supplementary Table 2.

Figure 5. EDAC and EPLIN act upstream of the Warburg effect-like metabolic changes in RasV12 cells surrounded by normal cells. (**a**) TMRM incorporation in EPLIN-knockdown RasV12-transformed cells. MDCK-pTR GFP-RasV12 cells or MDCK-pTR GFP-RasV12 EPLIN-shRNA1 cells were co-cultured with normal MDCK cells and loaded with 50 nM TMRM. (**b**) Quantification of the fluorescence intensity of TMRM. Data are mean ± s.e.m.. Values are expressed as a ratio relative to MDCK. **P*<0.001, unpaired two-tailed t-test; n=64, 21 and 45 cells pooled from two independent experiments. (**c**) Effect of EPLIN-knockdown on the mRNA level of PDK4 in RasV12 cells surrounded by normal cells. MDCK-pTR GFP-RasV12 cells or MDCK-pTR GFP-RasV12 EPLIN-shRNA1 cells were co-cultured with normal MDCK cells or cultured alone. GFP-positive RasV12 cells were selectively collected by FACS sorting and subjected to qPCR analysis. Values are shown as fold change in RasV12 cells surrounded by normal cells relative to RasV12 cells cultured alone. Data are mean ± s.e.m.. **P*<0.05, unpaired two-tailed t-test; n= three independent experiments. (**d**) Effect of EPLIN-knockdown on PDH phosphorylation or LDHA accumulation. MDCK-pTR GFP-RasV12 cells or MDCK-pTR GFP-RasV12 EPLIN-shRNA1 cells were co-cultured with normal MDCK cells. Cells were stained with Hoechst 33342 (blue) and anti-p-PDH or anti-LDHA antibody (red). (**e**) TMRM incorporation in RasV12-transformed cells surrounded by Filamin-knockdown cells. MDCK-pTR GFP-RasV12 cells were co-cultured with MDCK cells or MDCK-pTR Filamin-shRNA1 cells, and loaded with 50 nM TMRM. (**f**) Quantification of the fluorescence intensity of TMRM. Data are mean ± s.e.m.. Values are expressed as a

ratio relative to MDCK. *P<0.001, unpaired two-tailed t-test; n= 50, 41 and 42 cells pooled from three independent experiments. (**g**) Effect of Filamin-knockdown in the surrounding normal cells on PDH phosphorylation or LDHA accumulation in RasV12-transformed cells. MDCK-pTR GFP-RasV12 cells were co-cultured with MDCK-pTR Filamin-shRNA1 cells. Cells were stained with Hoechst 33342 (blue) and anti-p-PDH or anti-LDHA antibody (red). Scale bars, 10 μm (**a**, **d**, **e**, **g**). Statistics source data for **b**, **c**, **f** are provided in Supplementary Table 2.

Figure 6. FRET analyses for intracellular glucose. (**a**) Schematics for Glucose-FRET. (**b**) Glucose-FRET images. MDCK-pTRE3G myc-RasV12 cell lines stably expressing FLII^{12}Pglu-700μδ6 (RasV12 Glu-FRET No. 1 or No. 2) were co-cultured with MDCK cells or cultured alone with doxycycline for 16 h and then analysed by dual-emission fluorescence microscopy. FRET/CFP ratio images were generated to represent FRET efficiency. Scale bars, 10 μm. (**c**) Quantification of Glucose-FRET efficiency (FRET/CFP). The box plots represent values from the 25th (bottom) to the 75th (top) percentiles, with the median as the horizontal line. *P<0.001, unpaired two-tailed t-test; n=40, 61, 41 and 68 cells pooled from three independent experiments. Statistics source data for **c** are provided in Supplementary Table 2.

Figure 7. PDK-mediated mitochondrial dysfunction induces apical elimination of RasV12-transformed cells *ex vivo*. (**a**) Strategy for the establishment of the cell competition mouse model. (**b**) Immunofluorescence images of intestinal organoids from *Villin-Cre^{ERT2};LSL-RasV12-IRES-eGFP* or *;LSL-eGFP* mice after treatment of 100 nM tamoxifen. The areas in the white boxes are shown at higher magnification in the lower panels. ‘Extruding’; with their nucleus apically shifted, but still attached to

the basement membrane. ‘Extruded’; completely detached from the basement membrane and translocated into the apical lumen. Data are mean ± s.e.m.. *P<0.001 for extruded + extruding between RasV12-GFP- and GFP-expressing cells, unpaired two-tailed t-test; n=three independent experiments, each having 153, 259, 197 and 244 cells quantified for Villin-RasV12 and n=194, 288, 312 and 239 cells quantified for Villin-GFP. (**c**) Immunofluorescence images of intestinal organoids from *villin-Cre^{ERT2};LSL-RasV12-IRES-eGFP* mice at 24 h after 1 μM tamoxifen treatment. The arrow and arrowhead indicate an apically extruding RasV12 cell and the cluster of several RasV12 cells that are not extruded and remain within the epithelium, respectively. For quantification, the clusters are categorized by the number of RasV12 cells present in each cluster. Data are mean ± s.e.m.. n=three independent experiments, each having 149, 188 and 191 cells quantified. (**d**-**f**) TMRM incorporation (**d**, **e**) or immunofluorescence of p-PDH (**f**) in intestinal organoids from *villin-Cre^{ERT2};LSL-RasV12-IRES-eGFP* or *;LSL-eGFP* mice at 24 h after tamoxifen treatment. Arrows indicate RasV12-transformed cells with elevated PDH phosphorylation. (**e**) Quantification of the fluorescence intensity of TMRM. Data are mean ± s.e.m.. *P<0.001, unpaired two-tailed t-test; n=71, 37, 30 and 28 cells pooled from three independent experiments. (**g**, **h**) Effect of DCA on apical extrusion *ex vivo*. (**g**) Intestinal organoids from *villin-Cre^{ERT2};LSL-RasV12-IRES-eGFP* mice were treated with 100 nM tamoxifen and cultured for 24 h in the absence or presence of DCA. Asterisks in the images indicate mucin-rich, autofluorescent materials in the apical lumen (**b**-**d**, **f**, **g**). Ba and Ap stand for the basal and apical side, respectively (**b**-**d**, **f**, **g**). Scale bars, 10 μm (**b**-**d**, **f**, **g**). (**h**) Quantification of the effect of DCA on apical extrusion *ex vivo*. Data are mean ± s.e.m.. *P<0.005, unpaired two-tailed t-test; n=two

or three independent experiments, each having 157 and 217 cells quantified. Statistics source data for **b**, **c**, **e**, **h** are provided in Supplementary Table 2.

Figure 8. PDK-mediated mitochondrial dysfunction induces apical elimination of RasV12-transformed cells *in vivo*. (**a**) Immunofluorescence images of intestinal villi from *Villin-Cre^{ERT2};LSL-eGFP* or *;LSL-RasV12-IRES-eGFP* mice after tamoxifen injection. Note that apicobasal polarity is reversed between *ex vivo* and *in vivo*. (**b**) 'Not extruded'; remaining within the epithelium. 'Apical extruding'; with their nucleus apically shifted, but still attached to the basement membrane. 'Apical extruded'; completely detached from the basement membrane and translocated into the apical lumen. An arrow indicates 'Basal extruding'; basally delaminated beneath the basement membrane. (**c**) Quantification of the apical and basal extrusion. Data are mean ± s.e.m.. *P<0.05 for extruded + extruding between GFP- and RasV12-GFP-expressing cells, unpaired two-tailed t-test; n=two independent experiments, each having 958, 772, 532 and 605 cells quantified for Villin-GFP mice and n=253, 308, 80 and 92 cells quantified for Villin-RasV12 mice. (**d**) Intravital two-photon imaging of the small intestine of *Villin-Cre^{ERT2};LSL-RasV12-IRES-eGFP* mice. The arrowhead indicates an apically extruding cell. Scale bar, 50 μm. (**e**) *villin-Cre^{ERT2};LSL-RasV12-IRES-eGFP* or *;LSL-eGFP* mice pre-treated with or without DCA were injected with tamoxifen and sacrificed 3 days later while DCA was continuously administrated during this period. Arrowheads indicate apically extruding or extruded cells. (**f**) Quantification of the effect of DCA on apical extrusion *in vivo*. Data are mean ± s.e.m.. *P<0.01, unpaired two-tailed t-test; n=two or three independent experiments, each having 306, 496, 384 and 260 cells quantified. (**g**) An iGT operated mouse. The dotted line indicates the iGT-operated intestinal region. (**h**) Immunofluorescence

images of iGT-operated intestinal villi with or without Cy3-siRNA-containing HVJ-E. Scale bars, 100 μm. (**i**) Effect of scramble- or PDK4-siRNA on expression of PDK4 in the iGT-operated intestinal epithelium. PDK4-knockdown is confirmed by western blotting. (**j**) Immunofluorescence images of intestinal villi from the non iGT-operated region and scramble- or PDK4-siRNA transfected region at 3 days after tamoxifen injection. Arrows indicate apically extruding or extruded cells. Scale bars, 10 μm (**a**, **b**, **e**, **j**). (**k**) Quantification of the apical and basal extrusion of RasV12-transformed cells. Data are mean ± s.e.m.. *P<0.01, unpaired two-tailed t-test; n= three independent experiments, each having 649, 413 and 338 cells quantified. For Fig. 8i, an unprocessed original scan of immunoblotting is also shown in Supplementary Fig. 9. Statistics source data for **c**, **f**, **k** are provided in Supplementary Table 2.

METHODS

Antibodies, plasmids and materials

The following antibodies were used in this study; goat anti-LDHA (sc-27230), mouse anti-Tom20 (sc-17764 clone F10) and mouse anti-EPLIN (sc-136399 clone 20) antibodies from Santa Cruz Biotechnology, mouse anti-myc (05-724 clone 4A6) and mouse anti-β-actin (MAB1501R clone C4) antibodies from Millipore, rabbit anti-phospho-PDH antibody (AP1062) from Calbiochem, mouse anti-PDH (ab110330 clone 9H9AF5) and chicken anti-GFP (ab13970) antibodies from Abcam, mouse anti-E-cadherin antibody (610181 clone 36) from BD Transduction and rabbit anti-PDK4 antibody (AP7041B) from ABGENT. Alexa-Fluor-568- and -647-conjugated phalloidin (Life Technologies) were used at 1.0 U ml^{-1}. Alexa-Fluor-568- and -647-conjugated secondary antibodies were from Life Technologies. Hoechst 33342 (Life Technologies) was used at a dilution of 1:5,000. TMRM, mitoSOX, MitoTracker Green and 2-NBDG (2-deoxy-2-[(7-nitro-2,1,3-benzoxadiazol-4-yl)amino]-D-glucose) were obtained from Molecular Probes. The following inhibitors, Radicicol (10 μM), (S)-(-)-blebbistatin (30 μM), KT5720 (4 μM), 3-MA (10 mM), Y27632 (20 μM) and Chrysin (100 μM) were from Calbiochem. L-NAME (300 μM) was from Santa Cruz, and Cytochalasin D (4 μM), NAC (5 mM), 2-DG (25 mM) and DCA (25 mM except for Fig. 7g, h and Supplementary Fig. 7c, d where 50 mM was used) were from Sigma-Aldrich.

Cell culture

MDCK cell lines were used in this study. Parental MDCK cell is the gift from Walter Birchmeier. The cell line was not found in the database of commonly misidentified cell lines that is maintained by ICLAC and NCBI Biosample. Mycoplasma

contamination is regularly tested for all cell lines in use using a commercially available kit (MycoAlert, Lonza). The cell lines were not further authenticated. MDCK, MDCK-pTR GFP-RasV12, MDCK-pTR cSrcY527F-GFP, MDCK-pTR Scribble-shRNA, MDCK-pTR GFP-RasV12 EPLIN-shRNA and MDCK-pTR Filamin A-shRNA cells were cultured as previously described[10, 14-16]. To establish MDCK -pTRE3G myc-RasV12 cells, cDNA of myc-H-RasV12 was cloned into Bam*H*I/Eco*R*I sites of pPB-TRE3G-MCS-CEH-rtTA3-IP, which was constructed by introducing the TRE3G promoter with cloning sites, insulator and rtTA3-expressing elements into a PiggyBac-based vector (SBI). MDCK cells were then transfected with pPB-TRE3G myc-RasV12 by nucleofection (nucleofector 2b Kit L, Lonza), followed by selection in medium containing 5 μg ml^{-1} blasticidin (Invitrogen). MDCK-pTRE3G myc-RasV12 cells stably expressing FLII[12]Pglu-700μδ6[49] were established by co-transfecting MDCK cells with pPB-TRE3G myc-RasV12 and pPB-FLII[12]Pglu-700μδ6 , followed by the same selection method as above. To establish MDCK-pTR GFP-RasV12 cells stably expressing PDK4-shRNA, LDHA-shRNA or Luciferase-shRNA, or MDCK cells stably expressing PDH-shRNA or Luciferase-shRNA in a tetracycline-inducible manner, each shRNA sequences were cloned into the *BglII* and *XhoI* site of pSUPER.neo+gfp (for the former three shRNAs) or pSUPERIOR.neo+gfp (for the latter two shRNAs)(Oligoengine). Sequences of shRNAs are listed in Supplementary Table 1. For tetracycline-inducible MDCK cell lines, 2 μg ml^{-1} of tetracycline (Sigma-Aldrich) was used to induce expression of proteins or shRNAs except for MDCK-pTRE3G myc-RasV12 cells for which 1 μg ml^{-1} of doxycycline (Sigma-Aldrich) was used. MDCK-pTR Filamin A-shRNA cells were incubated with tetracycline for 48 h to induce sufficient knockdown prior to co-incubation with MDCK-pTR GFP-RasV12 cells. For immunofluorescence, cells were

plated onto collagen gel-coated coverslips. Type-I collagen (Cellmatrix Type I-A) was obtained from Nitta Gelatin and was neutralized on ice to a final concentration of 2 mg ml^{-1} according to the manufacturer's instructions. The CellTracker dyes, CMTPX (red dye), CMFDA (green dye) and CMAC (blue dye) (Life Technologies) were used according to the manufacturer's instructions.

CRISPR/Cas9-based generation of PDK4 knockout cells

Guide sequences of PDK4 sgRNA1 and 2 targeting canis *PDK4* were designed on the exon 1 and 9, respectively, as described previously[50]. PDK4 sgRNA sequences (PDK4 sgRNA1, 5'-GCTTCGTGATGCGCAGCGC-3'; PDK4 sgRNA2, 5'-ACGGCACCAACGCCTGTGA-3') were introduced into the pCDH-EF1-Hygro-sgRNA vector[51] using primers listed in Supplementary Table 1. First, MDCK cells were infected with lentivirus carrying pCW-Cas9 as described[51], and were cultured in the 500 ng ml^{-1} puromycin-containing medium. The tetracycline-inducible MDCK-Cas9 cells were transfected with the pCDH-EF1-PDK4 sgRNA1 and 2 by nucleofection, followed by selection in medium containing 200 μg ml^{-1} of Hygromycin and subjected to limiting dilution. Indels on the *PDK4* exons in each monoclone were analysed by direct sequencing using primers listed in Supplementary Table 1. To generate PDK4-deleted cells carrying doxycycline-inducible GFP-RasV12, pPB-TRE3G GFP-RasV12 was introduced into the PDK4-deleted cells by nucleofection and antibiotics selection. In addition to the $PDK4^{-/-}$ MDCK-pTRE3G GFP-RasV12 cells, we generated $PDK4^{+/+}$ MDCK-pTRE3G GFP-RasV12 cells as a control cell line.

Mice

All animal experiments were conducted under the guidelines by the Animal Care Committee of Hokkaido University. The animal protocols were reviewed and approved by the Hokkaido University Animal Care Committee (Approval number:12-0116). We used 6-10 weeks old C57BL/6 mice of either sex. To establish *DNMT1*-CAG-*loxP*-STOP-*loxP*-HRas^{V12}-IRES-eGFP knock-in mice, the genomic fragments of DNA methyltransferase 1 (DNMT1) locus, the *loxP*-flanked stop and *neomycin resistance* cassette, cDNA encoding HRas^{V12} plus *frt*-flanked IRES-eGFP and *diphtheria toxin subunit A* gene were inserted into the targeting vector. The resulting plasmid DNA was linearized and electrophoretically transfected into IB10 ES cells. Recombinant alleles were verified by Southern blot analysis. The independent clones were each injected into blastcysts of C57BL/6 mice and were successfully transmitted through the germ-line, and *DNMT1*-CAG-*loxP*-STOP-*loxP*-HRas^{V12}-IRES-eGFP mice (acc. no. CDB0706K: http://www2.clst.riken.jp/arg/mutant%20mice%20list.html) were thus established. *Villin-Cre^{ERT2}* mice[52] were crossed with *DNMT1*-CAG-*loxP*-STOP-*loxP*-HRas^{V12}-IRES-eGFP mice or CAG-*loxP*-STOP-*loxP*-eGFP mice[53] to create Villin-RasV12-GFP or Villin-GFP mice respectively. Mice heterozygous for each transgene were used for experiments. For PCR genotyping of mice, primers listed in Supplementary Table 1 were used. The expected sizes of PCR products were 220 bp, 403 bp and 390 bp for *Villin-Cre^{ERT2}*, *DNMT1*-CAG-*loxP*-STOP-*loxP*-HRas^{V12}-IRES-eGFP and CAG-*loxP*-STOP-*loxP*-eGFP mice, respectively. For culturing intestinal organoids, isolated crypts from the mouse small intestine were entrapped in Matrigel (Corning) and plated in a non-coated 35-mm glass bottom dish as previously described[36]. The crypts embedded in Matrigel were covered with Advanced DMEM/F12 supplemented with N2 (Invitrogen), B27 (Invitrogen), 50 ng ml^{-1} EGF (Peprotech), 100 ng ml^{-1}

Noggin (Peprotech), 1.25 mM N-Acetylcystein (Sigma-Aldrich) and R-spondin conditioned medium collected from 293T-HA-Rspol-Fc cells kindly provided by Dr. Calvin Kuo (Stanford University). After 96 h culture, organoids were incubated with tamoxifen (Sigma) for 24 h to induce transgenes. Subsequently, tamoxifen was washed out, and organoids were cultured for the indicated times for analyses. For *in vivo* experiments, 6-10 weeks old Villin-RasV12-GFP or Villin-GFP mice were given a single intraperitoneal injection of 2 mg of tamoxifen in corn oil (Sigma), and were then sacrificed at 2, 3, 5 or 7 days after Cre activation. To examine the effect of DCA, the mice were first pretreated with 5.0 g l^{-1} DCA in the drinking water for 2 weeks. Subsequently, the mice were injected intraperitoneally with 2.0 mg of tamoxifen and sacrificed 3 days later while DCA was continuously administrated during this period. The iGT (intestine-specific gene transfer) experiments were performed as previously described[37]. Briefly, 3-5 cm regions of small intestine drawn out from the peritoneal cavity were tied with nylon string. 300 μl of the mucus removing solution (20 mM DTT, 0.05% Tween-20 in PBS) was injected into the intestinal lumen for 15 min, removed and incubated with the same solution for 10 min. After washing with PBS three times by pipetting, 300 μl of the transfection solution containing Cy3-labelled siRNA and HVJ-E (haemagglutinating virus of Japan envelope) was injected, and the mice were left for 1 h. The sequences of Scramble- and PDK4-siRNA are listed in Supplementary Table 1. 2.0 mg of tamoxifen was injected into the peritoneal cavity when the wound was sutured. The mice were sacrificed for the analysis after 3 days of iGT.

Immunofluorescence and western blotting

For immunofluorescence, MDCK-pTR GFP-RasV12, MDCK-pTR cSrcY527F-GFP, MDCK-pTR Scribble-shRNA, MDCK-pTRE3G myc-RasV12, MDCK-pTR GFP-RasV12 PDK4-shRNA, MDCK-pTRE3G GFP-RasV12 PDK4-sgRNA, MDCK-pTR PDH-shRNA, MDCK-pTR GFP-RasV12 EPLIN-shRNA, MDCK-pTR GFP-RasV12 LDHA-shRNA or MDCK-pTR GFP-RasV12 Luciferase-shRNA cells were mixed with MDCK, MDCK-pTR Filamin A-shRNA or MDCK-pTR Luciferase-shRNA cells at a ratio of 1:50 and plated onto collagen-coated coverslips as previously described[10]. The mixture of cells was incubated for 8-12 h, followed by tetracycline or doxycycline treatment for 16 h, except for analyses of apical extrusions that were examined after 24 h of tetracycline or doxycycline addition. Cells were fixed with 4% paraformaldehyde (PFA) in PBS and permeabilised as previously described[11]. All primary antibodies were used at 1:100, and all secondary antibodies were used at 1:200. To monitor the mitochondrial activity or superoxide production, cells were loaded with 50 nM TMRM or 5 μM MitoSOX respectively for 30 min and subjected to microscopic observation or quantitatively analysed by CellInsight^{TM} image cytometer (Thermo Fisher Scientific). As to TMRM, we have thoroughly checked and optimized the experimental conditions. After titration of TMRM concentration, we chose 50 nM that provides clear and sufficient fluorescence intensity. By checking the effect of oligomycin and FCCP, we confirmed that the experimental condition is under the non-quenching mode using 50 nM TMRM[54]. We also confirmed that 2 μg ml^{-1} tetracycline did not affect TMRM fluorescence. The ratiometric images of TMRM and MitoTracker Green were obtained by incubating cells with 200 nM MitoTracker Green for 2 h, briefly washed, and then loaded with 50 nM TMRM. The 2-NBDG uptake was examined by incubating cells with glucose-free DMEM for 2 h followed by addition of 100 μM 2-NBDG for 30 min. For immunofluorescence using

intestinal organoids, cells grown in matrigels were incubated with Cell Recovery Solution (Corning) for 8 min before fixation with 4% PFA. After fixation, cells were permeabilised in 0.5% Triton X-100/PBS for 1 h and blocked in 1% BSA/PBS for 1 h. For immunohistochemical examinations of the small intestine, the tissues were isolated and fixed in 4% PFA, dehydrated, and embedded in paraffin. Microsections of each specimen were placed on glass slides, de-paraffinized and processed for immunostaining. The iGT-operated small intestine was embedded in OCT compound (Tissue-Tek), and frozen sections (10 μm) were cut on a cryostat. Immunofluorescence images were analysed by the Olympus FV1000 or FV1200 system and Olympus FV10-ASW software. Images were quantified by the MetaMorph software (Molecular Devices). Western blotting was performed as previously described[55]. Primary antibodies were used at 1:1,000. The western blotting data were analysed using ImageQuant™ LAS4010 (GE Healthcare).

FRET analysis

Glucose-FRET experiments were performed as previously described[56]. In brief, MDCK-pTRE3G myc-RasV12 cells stably expressing FLII^{12}Pglu-700μδ6 were co-cultured with MDCK cells at a ratio of 1:50 or cultured alone on a collagen gel in 35-mm-diameter, glass-bottom dishes (Matsunami Glass). At 16 h after doxycycline addition, a differential interference contrast (DIC) image and CFP and FRET fluorescence images were recorded. FRET efficiency was calculated as a quotient of background-subtracted FRET and CFP images and is presented in an intensity-modified display mode with the MetaMorph software. In the intensity-modified display mode, eight colors from red to blue are used to represent the FRET efficiency. To evaluate ATP level, MDCK-pTRE3G myc-RasV12 cells were transiently

transfected with ATeam probe[57], stained with CMTPX, and were co-cultured with MDCK cells at ratio of 1:50 or cultured alone on a collagen gel in 35-mm-diameter, glass-bottom dishes. At 16 h after doxycycline addition, FRET efficiency was examined as described above.

Time-lapse microscopic observation

For *ex vivo* time-lapse analyses, intestinal organoids grown in matrigels were incubated with 100 nM tamoxifen for 24 h to induce transgenes. Subsequently, time-lapse observation was carried out for 24 h in the medium containing no tamoxifen by the Nipkow spinning disk confocal microscopy (X-Light; Crest Optics). Fluorescence images (853 x 720 pixels, 0.975-μm resolution) were captured at an exposure of 0.25 s. Images of 42-μm depth in the z-axis were obtained at 3-μm z-steps.

For intravital imaging of small intestine in living mice, mice were anesthetized with isoflurane, the small intestine was surgically exposed, and then villi were observed by using two-photon excitation microscopy. Intestinal lumen was visualized with 70-kDa tetramethylrhodamine-conjugated dextran (Sigma). Nuclei of cells were stained with intravenous injection of Hoechst33342 (Life Technologies) just before imaging. The imaging system was composed of a two-photon microscope (A1-MP; Nikon) driven by a laser (Chameleon Vision II Ti: Sapphire; Coherent) tuned to 880 nm and an inverted microscope equipped with a 20× objective lens (Plan Fluor; N.A., 0.75; Nikon). Fluorescent signals were detected through band-pass emission filters at 525/50 nm (for GFP) and at 575/25 nm (for tetramethylrhodamine). Raw imaging data were processed using the Imaris software (Bitplane).

Electron microscopy

MDCK-pTR GFP-RasV12 cells were cultured alone or co-cultured with MDCK cells in collagen gel-coated, grid-imprinted plastic dishes (μ-Dish 35-mm Grid-500, Ibidi Corporation). After tetracycline treatment for 24 h, cells were fixed in 2% glutaraldehyde in HEPES buffer (30 mM HEPES, 0.1 M NaCl and 2 mM $CaCl_2$ (pH 7.4)), and fluorescence and DIC images of GFP-RasV12 cells and the surrounding cells were captured together with the underlying, numbered grid information. Cells were then post-fixed in 2% osmium tetroxide in 0.1 M imidazole (pH 7.4) and stained with 1% uranyl acetate (UA) before being dehydrated and embedded in Araldite-Epon resin (Electron Microscopy Sciences). During these procedures, GFP fluorescence was lost, but the grid was imprinted onto the resin. Subsequently, GFP-RasV12 cells and the 2 or 3 rows of surrounding MDCK cells were selected and excised, while referring to the grid information, morphology of the cells and the captured images. Ultrathin sections of the trimmed sample were poststained with UA and lead citrate, and cells were imaged with an electron microscope (JEM-1400; JEOL Corporation) operating at 80 kV.

Quantitative real-time PCR

MDCK-pTR GFP-RasV12 cells or 10:1 mix culture of MDCK and MDCK-pTR GFP-RasV12 cells were cultured at a density of $2x10^7$ cells on the collagen-coated 15-cm dishes (Greiner-Bio-One). After incubation with tetracycline for 16 h, GFP-positive RasV12 cells and GFP-negative MDCK cells were separated with an analytical flow cytometer. Total RNA was extracted from the isolated cells using Trizol® (Thermo Fisher Scientific) and the RNeasy Mini Kit (QIAGEN) and reverse transcribed using QuantiTect Reverse Transcription Kit (QIAGEN). GeneAce SYBR qPCR Mix (NIPPON GENE) was used to perform qPCR using the StepOne™ system (Thermo

Fisher Scientific). The primer sequences used are listed in Supplementary Table 1. We used β-actin as a reference gene to normalise data.

Lactate assay

For lactate assay, MDCK cells, MDCK-pTR GFP-RasV12 cells, MDCK-pTR GFP-RasV12 LDHA-shRNA cells or 1:1 mix of MDCK and MDCK-pTR GFP-RasV12 or MDCK-pTR GFP-RasV12 LDHA-shRNA cells were cultured at a density of $6.5x10^5$ cells on the collagen-coated 12-well dishes (Falcon) in DMEM containing neither phenol red nor fetal calf serum. The culture medium was replaced with fresh medium at 12 h after tetracycline addition and collected 12 h later. Samples were subjected to measurement of lactate concentration using Lactate Assay kit (BioVision).

HIF1 reporter assay

MDCK or MDCK-pTR GFP-RasV12 cells were co-transfected with pCDH/5HRE-Luc (kindly provided by Dr. Hiroshi Harada (Kyoto University)) and pRL-TK. After 24 h, cells were trypsinised, and cultured alone or co-cultured with the indicated cells (total cell number: $3.5x10^5$) for 8 h, followed by tetracycline treatment for 16 h. Firefly luciferase activity was measured using Dual-Lucifease Reporter assay (Promega) and normalized by Renilla luciferase activity.

Statistics and reproducibility

For data analyses, unpaired two-tailed Student's *t*-tests were used to determine *P*-values. *P*-values less than 0.05 were considered to be significant. No statistical method was used to predetermine sample size. For animal studies, the experiments were not randomized, and the investigators were not blinded to allocation during

experiments. All results were reproduced at least two independent experiments and at least three mice of each genotype. Western blots and immunofluorescence microscopy were independently repeated at least twice. All representative microscopy images are presented with quantification of the entire data set. Detailed information on replication of experiments can be found in the corresponding legends.

Data availability

Source data for Fig. 1b, f, 2b, d, f, 3a, c, e, g, i, 4c, e, 5b, c, f, 6c, 7b, c, e, h, 8c, f, k and Supplementary Fig. 1e, h, 3l, n, 4c, g, 5f, g, i, 6c, 7d, e have been provided as Supplementary Table 2. All data supporting the findings of this study are available from the corresponding author on request.

Supplementary Figure 1. The mitochondrial membrane potential is decreased in Src-transformed cells but not in Scribble-knockdown cells when they are surrounded by normal cells. (**a**) TMRM incorporation in Src-transformed cells. MDCK-pTR cSrcY527F-GFP cells were mixed with normal MDCK cells or cultured alone, and loaded with 50 nM TMRM (red). Arrows indicate Src-transformed cells showing diminished fluorescence intensity of TMRM. (**b**) TMRM incorporation in Scribble-knockdown cells. MDCK-pTR Scribble-shRNA cells were mixed with normal MDCK cells or cultured alone, and incubated with tetracycline for 48 h and loaded with 50 nM TMRM (red). Arrows indicate Scribble-knockdown cells showing the comparable fluorescence intensity of TMRM to that in the surrounding normal cells. (**c**) Establishment of doxycycline-inducible myc-RasV12 MDCK cell lines. Doxycline-induced expression of myc-RasV12 protein is determined by western blotting. (**d**) Immunofluorescence images of xz sections of myc-RasV12 MDCK cells surrounded by normal MDCK cells. (**e**) Quantification of the apical extrusion of myc-RasV12 cells. Data are mean ± s.e.m.. n=two independent experiments, each having 171, 191 and 243 cells quantified. These data demonstrate that myc-RasV12 cells are apically extruded when surrounded by normal cells, similarly for GFP-RasV12 cells. (**f**) TMRM incorporation in myc-RasV12 cells. MDCK-pTRE3G myc-RasV12 cells were fluorescently labelled with CMFDA dye (green), and co-cultured with normal MDCK cells or cultured alone, and loaded with 50 nM TMRM (red). This result shows that non-cell-autonomous reduction of TMRM incorporation also occurs in myc-RasV12 cells. (**g**) Immunofluorescence and ratiometric images of MitoTracker Green (MTG) and TMRM. MDCK-pTRE3G myc-RasV12 cells were fluorescently labelled with CMAC dye (blue), and co-cultured with normal MDCK cells or cultured alone. Cells were incubated with 200 nM MTG for 2 h, washed briefly and

subsequently loaded with 50 nM TMRM for 30 min. Scale bars, 10 μm (**a**, **b**, **d**, **f**, **g**). (**h**) Quantification of the ratio of TMRM to MTG. Data are mean ± s.e.m.. *P<0.001, unpaired two-tailed t-test; n=50 and 36 cells pooled from three independent experiments. For Supplementary Fig. 1c, unprocessed original scans of immunoblotting are also shown in Supplementary Fig. 9. Statistics source data for **e**, **h** are provided in Supplementary Table 2.

Supplementary Figure 2. Mitophagosome-like structures are frequently observed in RasV12 cells that are surrounded by normal epithelial cells. Electron microscopic images of MDCK-pTR GFP-RasV12 cells cultured alone or surrounded by normal cells. The areas in the white boxes are shown below at higher magnification, demonstrating mitophagosome-like structures. In RasV12 cells surrounded by normal cells, on average 0.65 mitophagosome-like structures in a single RasV12 cell per slice (51 slices); in RasV12 cells cultured alone, on average 0.01 mitophagosome-like structures in a single RasV12 cell per slice (84 slices). Scale bars, 2 μm (upper panels) and 0.5 μm (lower panels).

Supplementary Figure 3. Knockdown/knockout of PDK4 inhibits PDH phosphorylation and LDHA accumulation in RasV12-transformed cells surrounded by normal cells. (**a**) The illustration for the mode of action of PDK and LDHA. (**b**) A targeting scheme and DNA sequences of the wild type and PDK4-null MDCK-pTRE3G GFP-RasV12 cell lines. PAM motifs are underlined. The red spacing indicates a deleted nucleotide. (**c**-**n**) Effect of PDK4-knockdown or -knockout on p-PDH (**c**-**e**), TMRM incorporation (**f**, **g**), LDHA (**h**-**j**) or apical extrusion (**k**-**n**). MDCK-pTR GFP-RasV12 PDK4-shRNA cells (**c**, **h**), MDCK-pTR GFP-RasV12

Luciferase-shRNA cells (**d**, **f**, **i**) or MDCK-pTRE3G GFP-RasV12 PDK4-sgRNA cells (**e**, **g**, **j**) were mixed with normal MDCK cells or MDCK-pTR Luciferase-shRNA cells. Cells were loaded with 50 nM TMRM (**f**, **g**) or stained with Hoechst 33342 (blue) and anti-p-PDH (**c**-**e**) or anti-LDHA (**h**-**j**) antibody (red). (**g**) Note that PDK4-knockout rather promoted TMRM incorporation in RasV12 cells surrounded by normal cells. (**k**) Immunofluorescence images of xz sections of MDCK-pTR GFP-RasV12 Luciferase-shRNA cells surrounded by normal MDCK cells or of MDCK-pTR GFP-RasV12 cells surrounded by MDCK-pTR Lucifierase-shRNA cells. (**l**) Quantification of apical extrusion of RasV12 cells mixed with MDCK cells, RasV12 Luc-shRNA cells mixed with MDCK cells or RasV12 cells mixed with MDCK Luc-shRNA cells. Data are mean ± s.e.m.. *P<0.05, unpaired two-tailed t-test; n=three independent experiments, each having 340, 150 and 311 cells quantified. (**m**) Immunofluorescence images of xz sections of MDCK-pTRE3G GFP-RasV12 PDK4-sgRNA1 or -sgRNA2 cells surrounded by normal MDCK cells. Arrowheads indicate basal protrusions. (**n**) Quantification of the apical extrusion of MDCK-pTRE3G GFP-RasV12 PDK4-sgRNA1 or -sgRNA2 cells. Data are mean ± s.e.m.. Values are expressed as a ratio relative to MDCK:RasV12=50:1. *P<0.05, unpaired two-tailed t-test; n=three independent experiments, each having 240, 261 and 264 cells quantified. Scale bars, 10 μm (**c**-**k**, **m**). Statistics source data for **l**, **n** are provided in Supplementary Table 2.

Supplementary Figure 4. PDK inhibitor Radicicol restores TMRM incorporation and suppreses apical extrusion of RasV12-transformed cells surrounded by normal cells. (**a**) Effect of Radicicol on TMRM incorporation of RasV12-transformed cells. MDCK-pTR GFP-RasV12 cells were co-cultured with normal

MDCK cells in the absence or presence of 10 μM Radicicol and incubated with 50 nM TMRM. (**b**) Immunofluorescence images of xz sections of MDCK-pTR GFP-RasV12 cells surrounded by normal MDCK cells in the absence or presence of Radicicol. (**c**) Quantification of the effect of Radicicol on apical extrusion. Data are mean ± s.e.m.. *P<0.01, unpaired two-tailed t-test; n=three independent experiments, each having 323 and 230 cells quantified. (**d**) Effect of Radicicol on LDHA in RasV12-transformed cells that are surrounded by normal cells. MDCK-pTR GFP-RasV12 cells were mixed with normal MDCK cells in the absence or presence of Radicicol. Cells were stained with Hoechst 33342 (blue) and anti-LDHA antibody (red). (**e**) Establishment of MDCK-pTR GFP-RasV12 cells stably expressing LDHA-shRNA1 or -shRNA2. Knockdown of LDHA is confirmed by western blotting. (**f**) Effect of LDHA-knockdown on TMRM incorporation. MDCK-pTR GFP-RasV12 LDHA-shRNA1 or -shRNA2 cells were mixed with normal MDCK cells and loaded with 50 nM TMRM. (**g**) Quantification of the apical extrusion of MDCK-pTR GFP-RasV12 LDHA-shRNA1 or -shRNA2 cells. Data are mean ± s.e.m.. *P<0.05, unpaired two-tailed t-test; n=three independent experiments, each having 451, 436 and 449 cells quantified. (**h**) Establishment of tetracycline-inducible PDH-knockdown MDCK cell lines. Effect of tetracycline on expression of PDH protein is determined by western blotting. (**i**) TMRM incorporation in PDH-knockdown cells. MDCK-pTR PDH-shRNA1 or -shRNA2 cells were fluorescently labelled with CMFDA dye (green), and co-cultured with normal MDCK cells. Cells were incubated with tetracycline for 48 h, and loaded with 50 nM TMRM (red). (**j**) Immunofluorescence images of xz sections of MDCK-pTR PDH-shRNA cells surrounded by normal MDCK cells at 72 h after tetracycline addition. Scale bars, 10 μm (**a**, **b**, **d**, **f**, **i**, **j**). For Supplementary Fig. 4e, h, unprocessed original scans of immunoblotting are also

shown in Supplementary Fig. 9. Statistics source data for **c**, **g** are provided in Supplementary Table 2.

Supplementary Figure 5. Effect of various inhibitors on TMRM incorporation and FRET analyses for ATP. (**a**, **b**) Effect of EPLIN- or Filamin-knockdown on TMRM incorporation (**a**) or p-PDH and LDHA accumulation (**b**). MDCK-pTR GFP-RasV12 or MDCK-pTR GFP-RasV12 EPLIN-shRNA2 cells were co-cultured with MDCK or MDCK-pTR Filamin-shRNA2 cells. (**c**) MDCK-pTR GFP-RasV12 cells were co-cultured with normal MDCK cells in the presence of various inhibitors and loaded with TMRM (red). Each inhibitor inhibits the following molecule or cellular process; Blebbistatin: myosin-II, Cytochalasin D: actin polymerization, Y27632: Rho kinase, NAC: reactive oxygen species, L-NAME: nitrogen oxide synthase, 3-MA: autophagy, KT5720: PKA. (**d**) Schematics for ATP-FRET (ATeam). (**e**) ATP-FRET images. MDCK or MDCK-pTRE3G myc-RasV12 cells transiently expressing ATeam were stained with CMTPX and co-cultured with MDCK cells or cultured alone with doxycycline for 16 h in the absence or presence of DCA or 2-DG and then analysed by dual-emission fluorescence microscopy. FRET/CFP ratio images were generated to represent FRET efficiency. (**f**) Quantification of ATP-FRET efficiency ratio (FRET/CFP). The box plots represent values from the 25^{th} (bottom) to the 75^{th} (top) percentiles, with the median as the horizontal line. *P<0.001, unpaired two-tailed t-test; n=50, 34, 32, 32, 15 and 15 cells pooled from two independent experiments. (**g**) Effect of 2-DG on lactate production in RasV12-transformed cells. MDCK-pTRE3G myc-RasV12 cells were incubated with the indicated concentration of 2-DG for 24 h, and lactate concentration in the culture media was measured. Data are mean ± s.e.m. from three independent experiments. (**h**, **i**) Effect of 2-DG on apical extrusion of

RasV12-transformed cells. MDCK-pTR GFP-RasV12 cells were co-cultured with normal MDCK cells in the absence or presence of 25 mM 2-DG. (**h**) Immunofluorescence images of xz sections of MDCK-pTR GFP-RasV12 cells surrounded by normal MDCK cells in the absence or presence of 2-DG. (**i**) Quantification of the effect of 2-DG on apical extrusion. Data are mean ± s.e.m.. **P*<0.01, unpaired two-tailed t-test; n=three independent experiments, each having 341 and 328 cells quantified. Scale bars, 10 μm (**a**-**c**, **e**, **h**). Note that 2-DG could inhibit both oxidative and fermentative glucose metabolism. To further clarify the metabolic alterations during apical extrusion, additional experiments are required in future studies. Statistics source data for **f**, **g**, **i** are provided in Supplementary Table 2.

Supplementary Figure 6. Establishment of conditional RasV12-GFP knock-in mice and tamoxifen-dependent expression of transgenes in intestinal organoids. (**a**) Physical maps of the *DNMT1* gene locus and its targeting vector. The targeting vector contains a cDNA encoding H-RasV12 under control of the CAG promoter and downstream of a loxP-flanked stop cassette plus a frt-flanked IRES-eGFP component. Filled-in and open arrowheads indicate the loxP sequences and frt sequences, respectively. The grey rectangles under the line correspond to the probes that were used for Southern blot hybridization. Arrows denote PCR primer sites for the genotyping. (**b**) Southern blot analysis of genomic DNA prepared from the wild-type ES cells and the targeted ES clones. DNA was digested by *Bgl*II (probe 1) or *Sac*I (probe 2) and processed for Southern blotting using the hybridization probes shown in (**a**). (**c**) Organoids from *Villin-Cre^{ERT2};LSL-RasV12-IRES-eGFP* mice or *Villin-Cre^{ERT2};LSL-eGFP* mice were incubated with the indicated concentration of tamoxifen for 24 h and stained with Hoechst 33342 (blue). Ba and Ap stand for the

basal and apical side, respectively. Asterisks indicate mucin-rich, autofluorescent materials in the apical lumen. Scale bars, 10 μm. The percentage of RasV12-GFP- or GFP-expressing cells relative to total cells in an organoid was quantified. Data are mean ± s.e.m.. n=two independent experiments, each having 231, 245, 259 and 174 cells quantified for Villin-RasV12-GFP mice and 230, 244, 352 and 263 cells quantified for Villin-GFP mice. Statistics source data for **c** are provided in Supplementary Table 2.

Supplementary Figure 7. Cropped images of the time-lapse observation for apically extruding RasV12 cells in intestinal organoids. (**a**) Immunofluorescence of EPLIN in intestinal organoids from *villin-Cre^{ERT2};LSL-RasV12-IRES-eGFP* mice at 24 h after treatment of 100 nM or 1 μM tamoxifen. The organoids were stained with Hoechst 33342 (blue) and anti-EPLIN antibody (red). Scale bars, 10 μm. (**b**) Representative serial images of time-lapse microscopic observation for intestinal organoids from *Villin-Cre^{ERT2};LSL-eGFP* mice (upper panels) or *Villin-Cre^{ERT2};LSL-RasV12-IRES-eGFP* mice (middle and lower panels) at the indicated times after treatment of 100 nM tamoxifen. Note that apical extrusion of RasV12-transformed cells took variable times between 2-20 h. Scale bars, 50 μm. (**c**) Effect of DCA on TMRM incorporation *ex vivo*. The intestinal organoids from *Villin-Cre^{ERT2};LSL-RasV12-IRES-eGFP* mice at 24 h after treatment of 100 nM tamoxifen in the absence or presence of 50 mM DCA were loaded with 50 nM TMRM (red). Scale bars, 10 μm. Asterisks indicate mucin-rich, autofluorescent materials in the apical lumen (**a**, **c**). Ba and Ap stand for the basal and apical side, respectively (**a**-**c**). (**d**) Quantification of the fluorescence intensity of TMRM. Data are mean ± s.e.m.. Values are expressed as a ratio relative to normal DCA (-). *P<0.01, unpaired two-tailed t-test; n= 24, 25, 45

and 47 cells pooled from three independent experiments. (**e**) HIF1 reporter assay. MDCK cells or MDCK-pTR GFP-RasV12 cells were co-transfected with the HIF1 reporter and Renilla expression vector, and co-cultured with non-transfected MDCK cells or MDCK-pTR GFP-RasV12 cells in the absence or presence of 100 μM HIF1 inhibitor Chrysin. After 16 h incubation with tetracycline, cells were lysed and subjected to measurement of the luciferase activity. Data are mean ± s.e.m.. *P<0.05, unpaired two-tailed t-test; n= three independent experiments. Statistics source data for **d**, **e** are provided in Supplementary Table 2.

Supplementary Figure 8. A schematic model for molecular mechanisms of the Warburg effect-like metabolic changes in transformed cells that are surrounded by normal cells. (**a**) Effect of various inhibitors on apical extrusion of RasV12-transformed cells and on TMRM incorporation in RasV12-transformed cells that are surrounded by normal cells. *: statistically significant (unpaired two-tailed t-test); ND: not done; Grey box: our published observations[10, 11, 15, 16]. (**b**) Difference between conventional Warburg effect and EDAC-induced Warburg effect-like metabolic changes. (**c**) A schematic model for molecular mechanisms of the Warburg effect-like metabolic changes in transformed cells that are surrounded by normal cells.

Supplementary Figure 9. Unprocessed scans of original blots. Uncropped scans of images for all immunoblotting experiments are shown.

Supplementary Table 1. Sequences of primers, shRNAs, sgRNAs and siRNAs used in this study. Sequences of shRNAs, sgRNAs, siRNAs and primers used for genotyping and qPCR are shown.

Supplementary Table 2. Statistics source data. Statistics source data of all repeats are shown.

Supplementary Movie 1

GFP-expressing cells in the intestinal organoid epithelium.

This movie shows that GFP-expressing cells are not extruded from the intestinal organoid epithelium which is derived from *Villin-Cre^{ERT2};LSL-eGFP* mice. Time-lapse images were captured at 15-min intervals for 24 h.

Supplementary Movie 2

RasV12-GFP-expressing cells in the intestinal organoid epithelium.

This movie shows that RasV12-GFP-expressing cells are apically extruded from the intestinal organoid epithelium which is derived from *Villin-Cre^{ERT2};LSL-RasV12-IRES-eGFP* mice. Time-lapse images were captured at 15-min intervals for 24 h.

Supplementary Movie 3

RasV12-GFP-expressing cells in the intestinal organoid epithelium.

This movie shows that RasV12-GFP-expressing cells are apically extruded from the intestinal organoid epithelium which is derived from *Villin-Cre^{ERT2};LSL-RasV12-IRES-eGFP* mice. Time-lapse images were captured at 15-min intervals for 24 h.

Supplementary Movie 4

RasV12-GFP-expressing cells in the intestinal villi *in vivo*.

This intravital movie by two-photon imaging shows that RasV12-GFP-expressing cells are apically extruded from the intestinal villi which is derived from *Villin-Cre^{ERT2};LSL-RasV12-IRES-eGFP* mice. Time-lapse images were captured at 15-min intervals for 75 min.

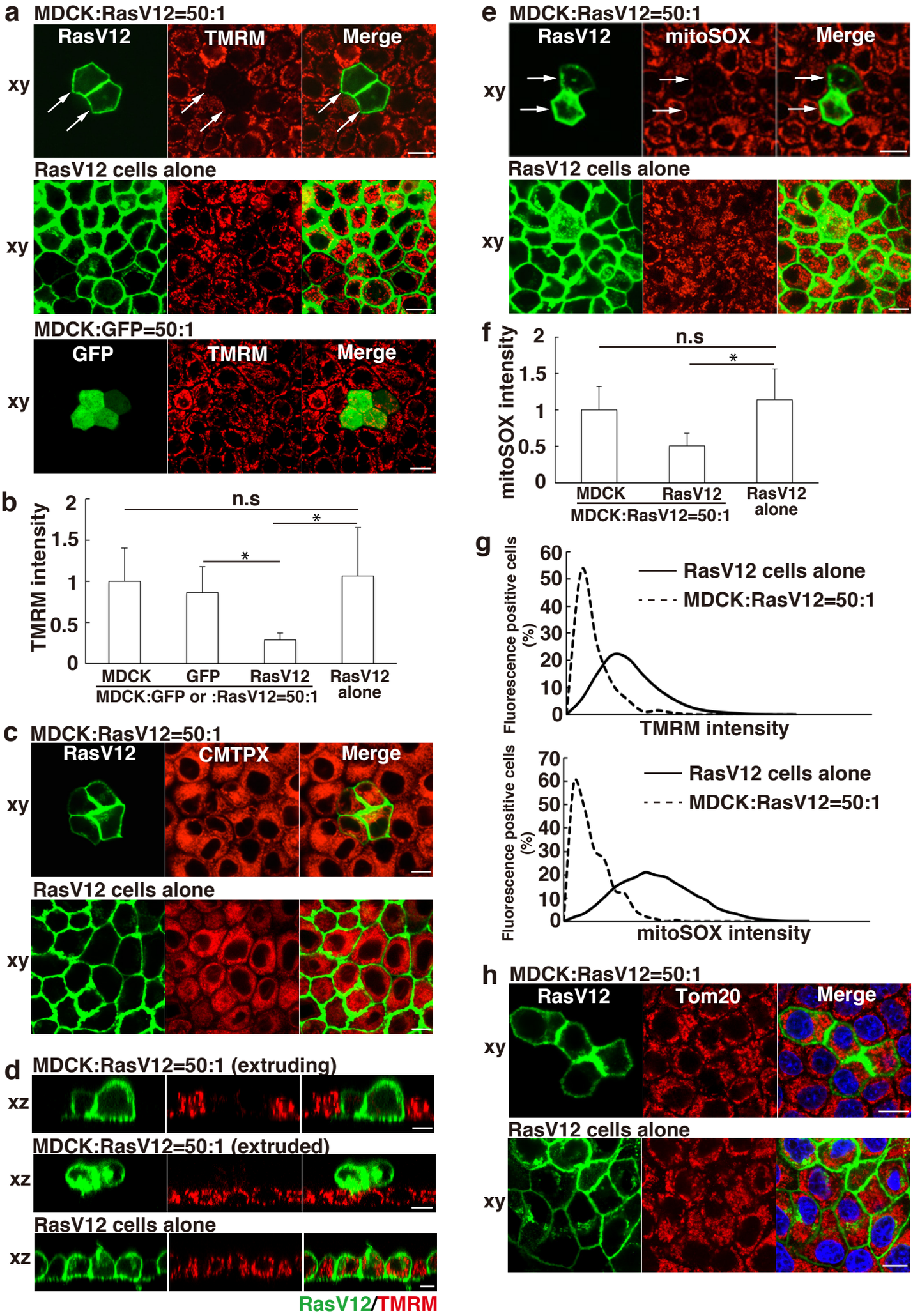

Figure 1 Kon et al.

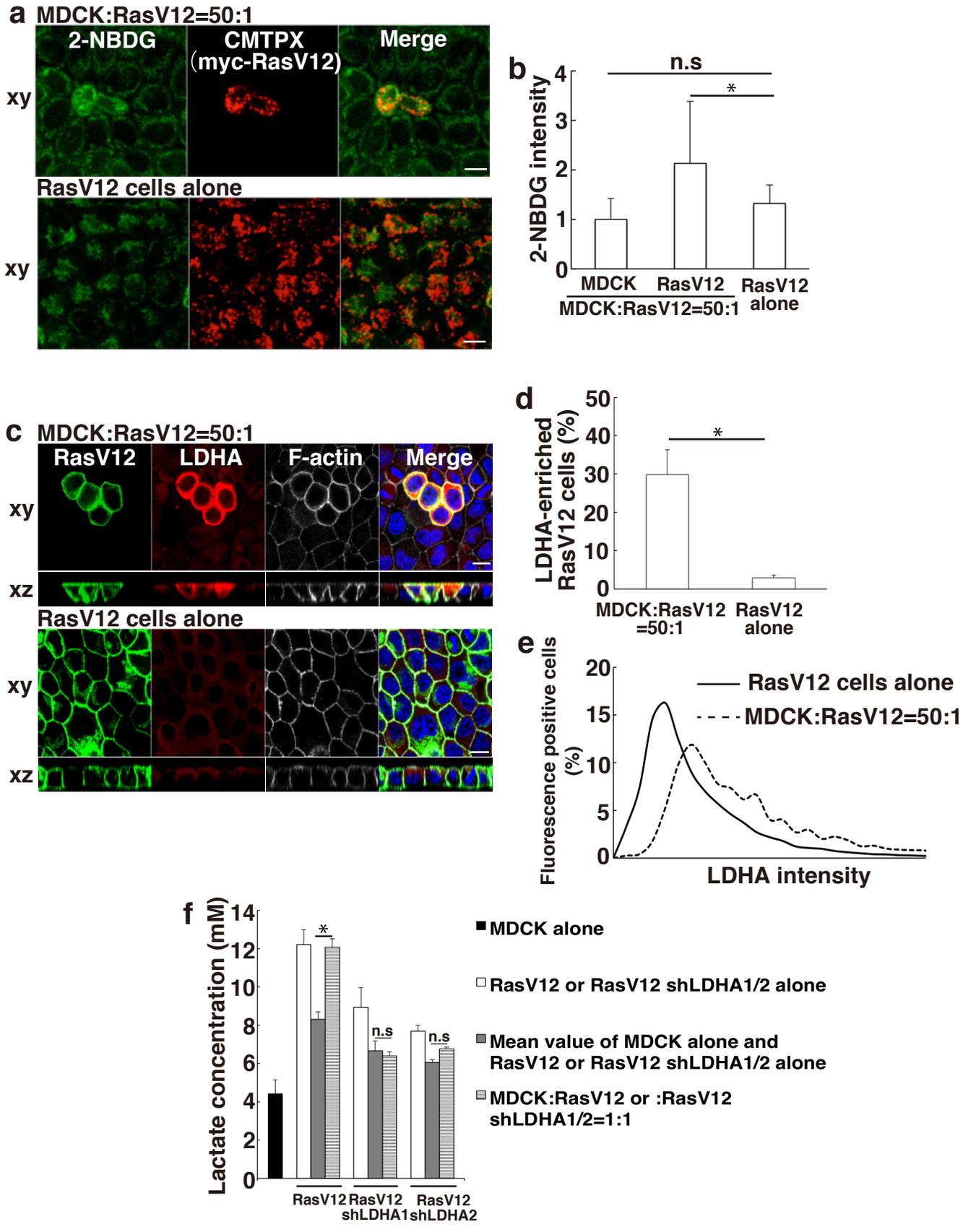

Figure 2 Kon et al.

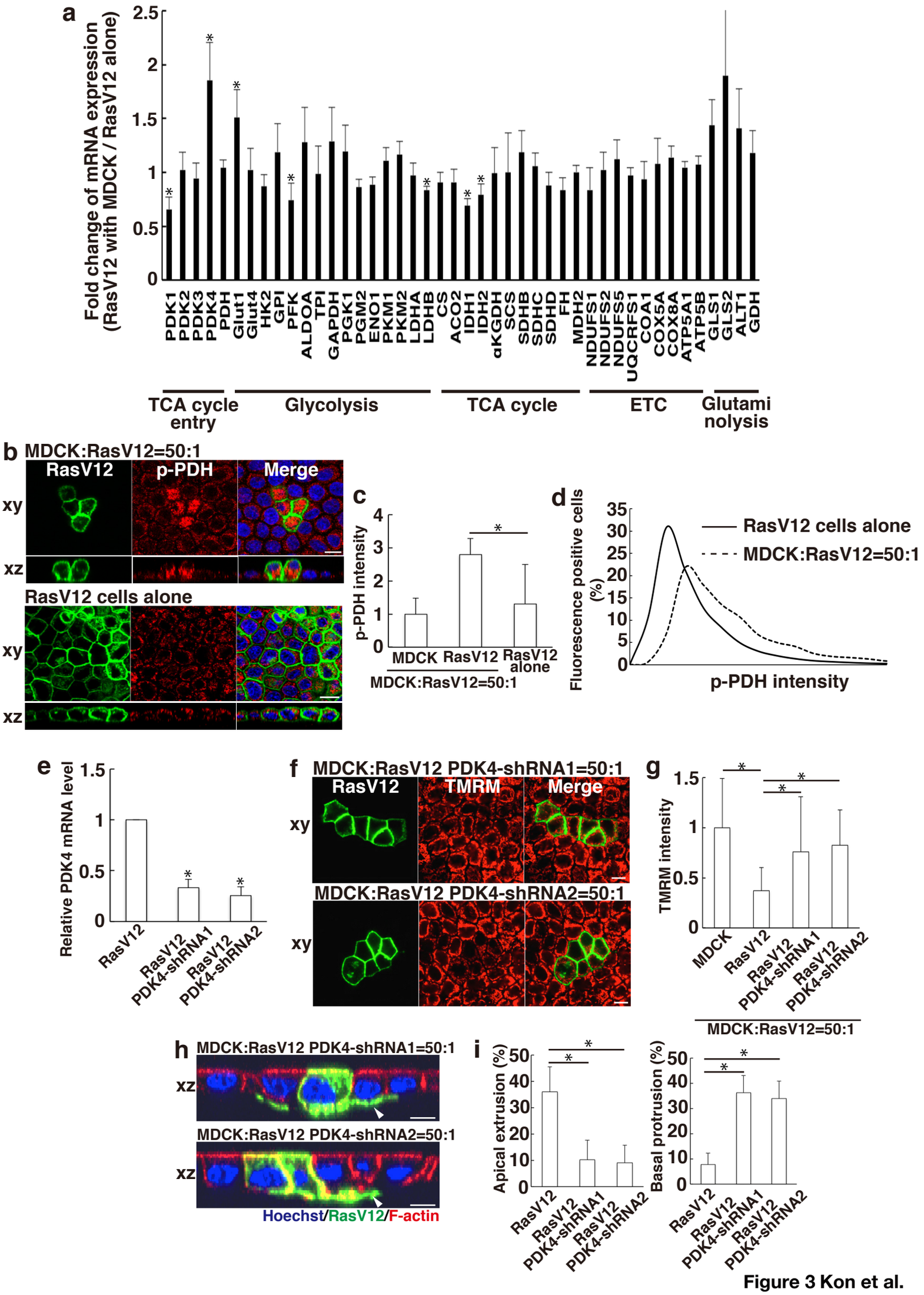

Figure 3 Kon et al.

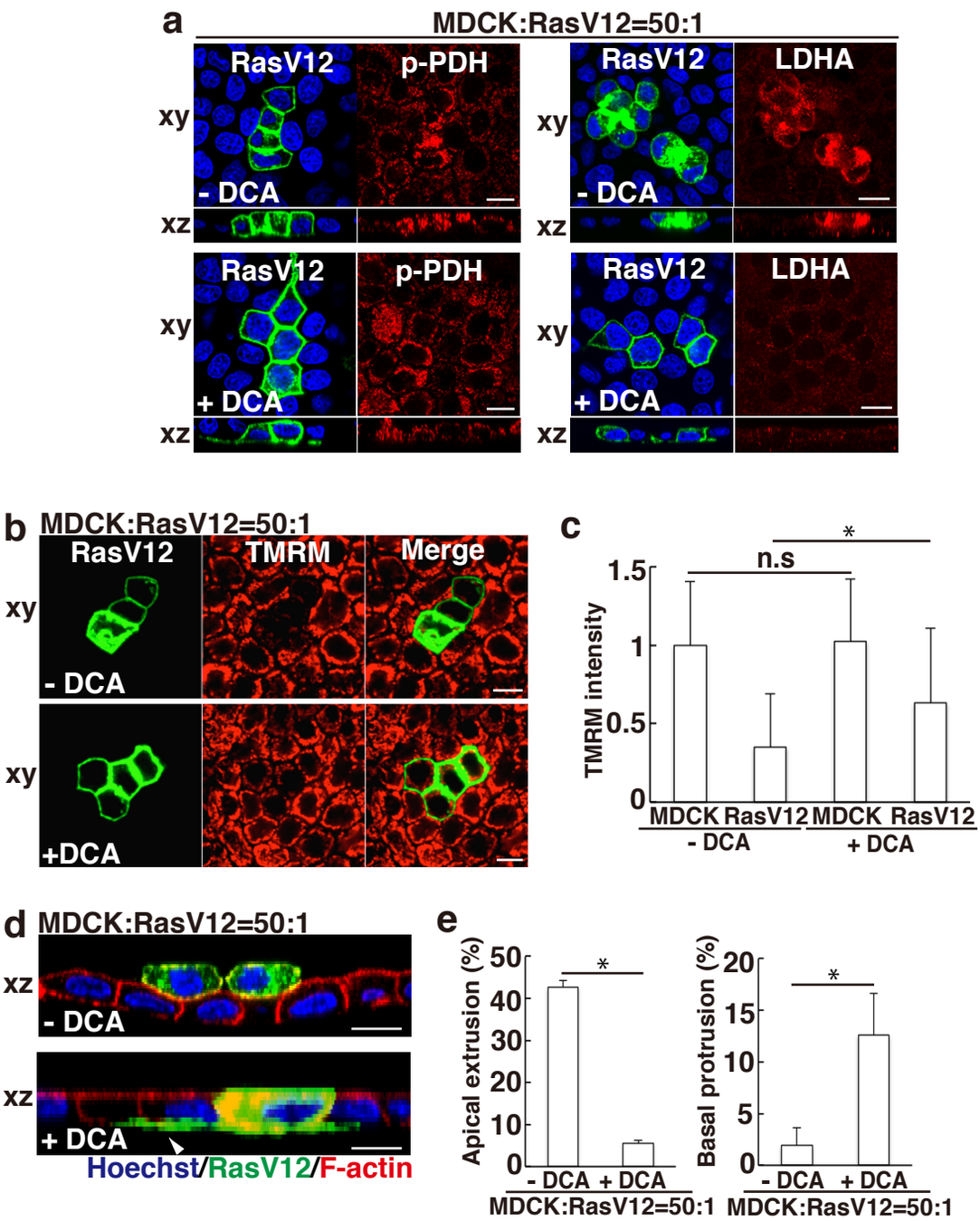

Figure 4 Kon et al.

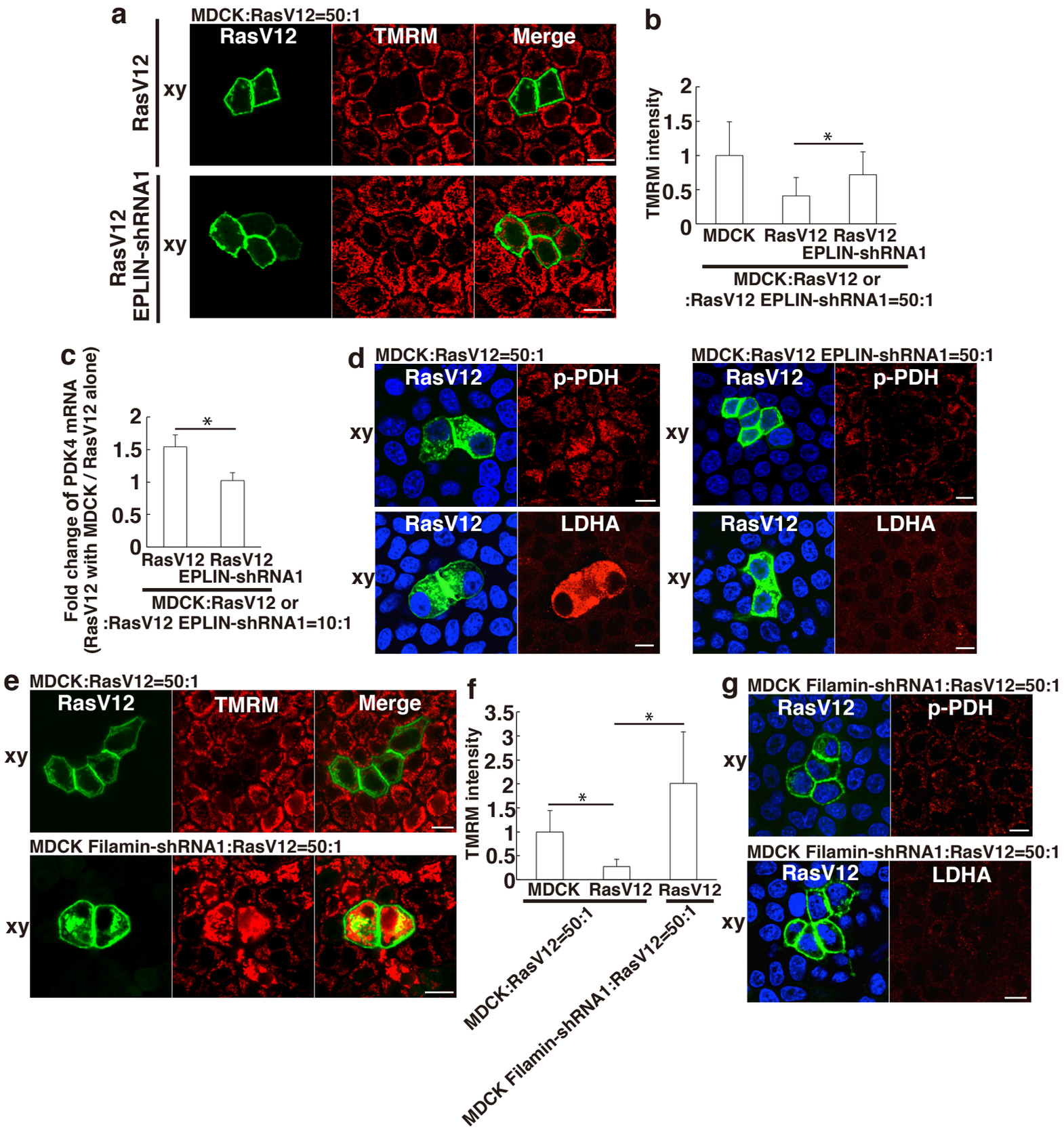

Figure 5 Kon et al.

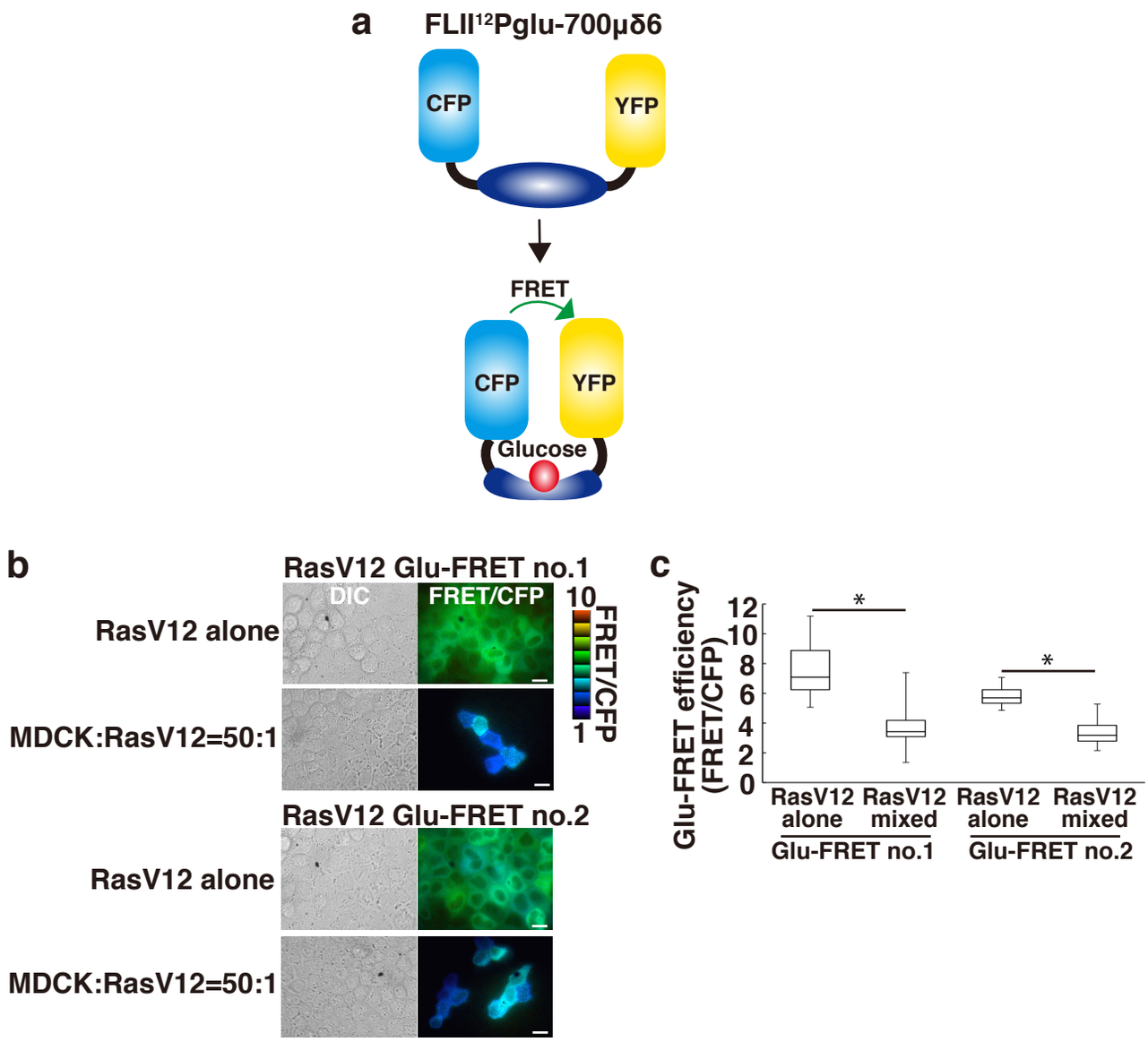

Figure 6 Kon et al.

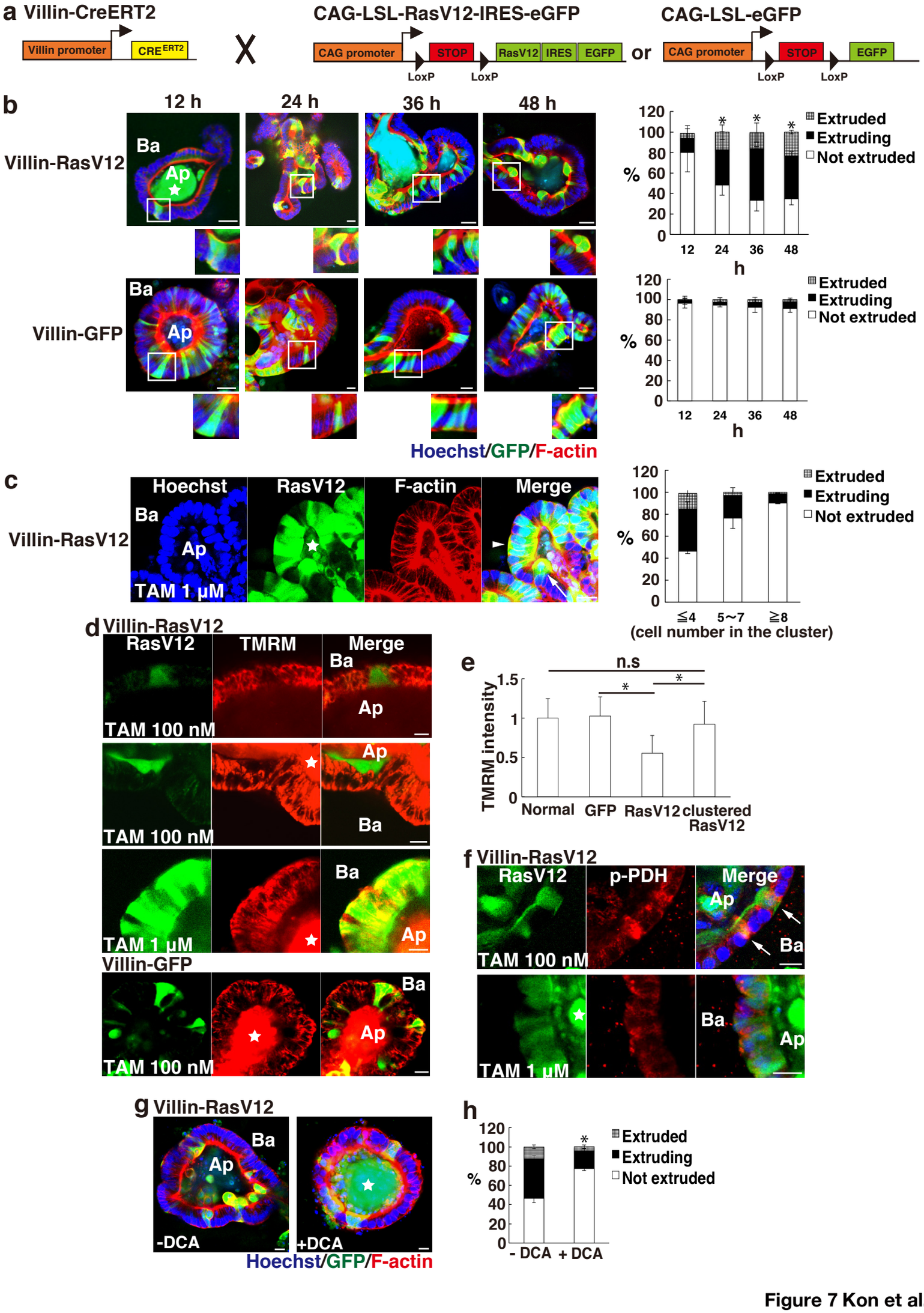

Figure 7 Kon et al.

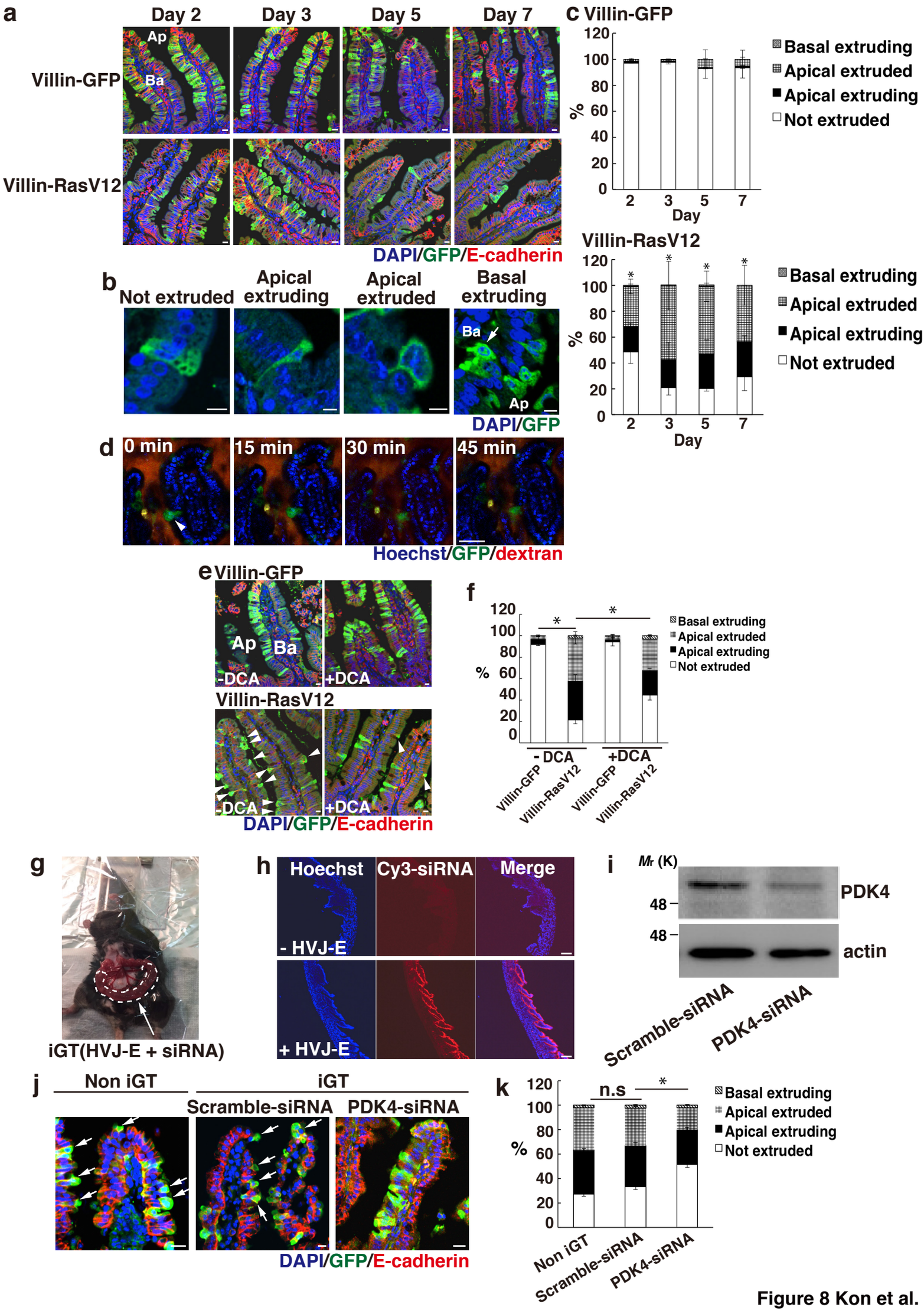

Figure 8 Kon et al.

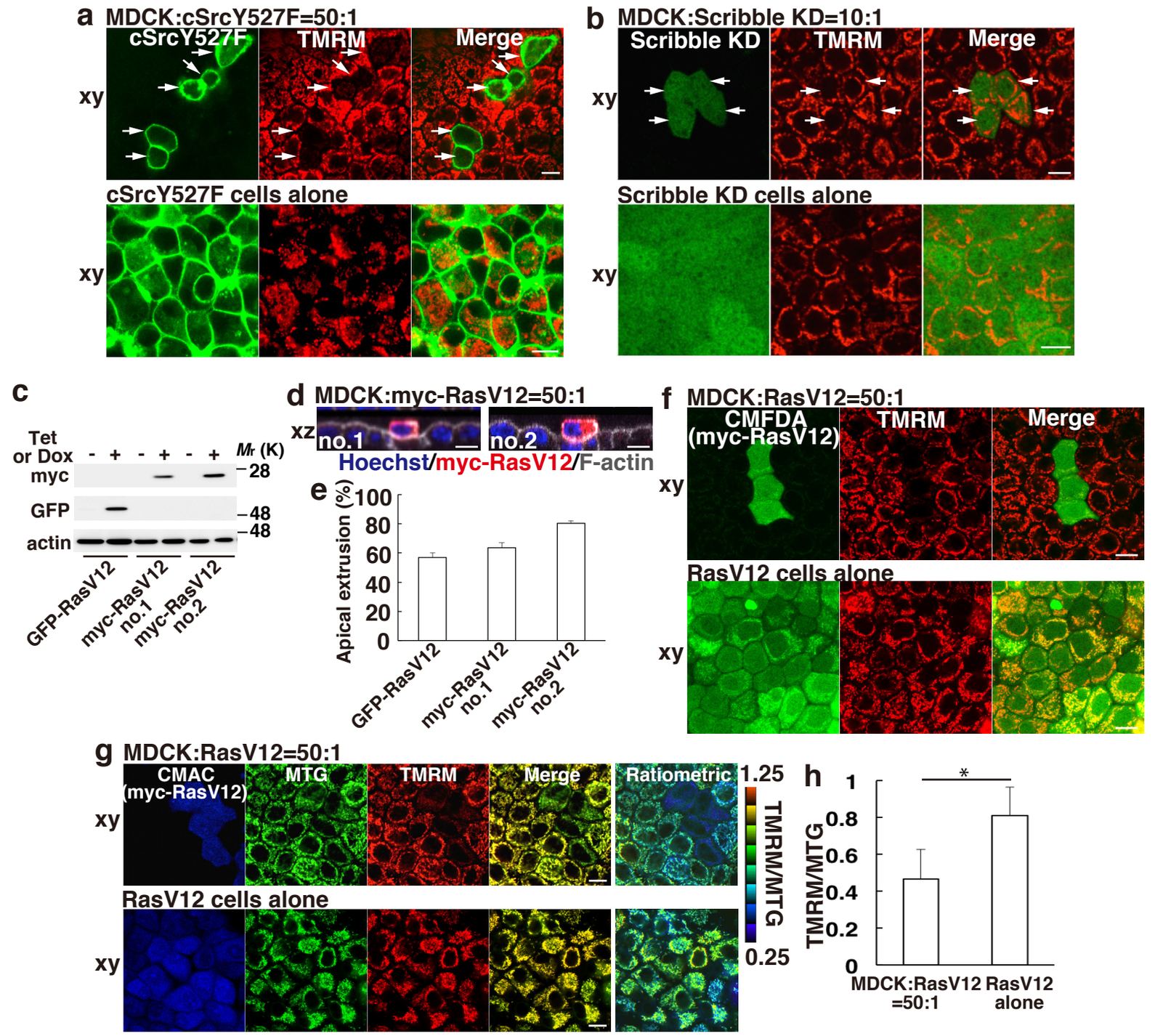

Supplementary Figure 1 Kon et al.

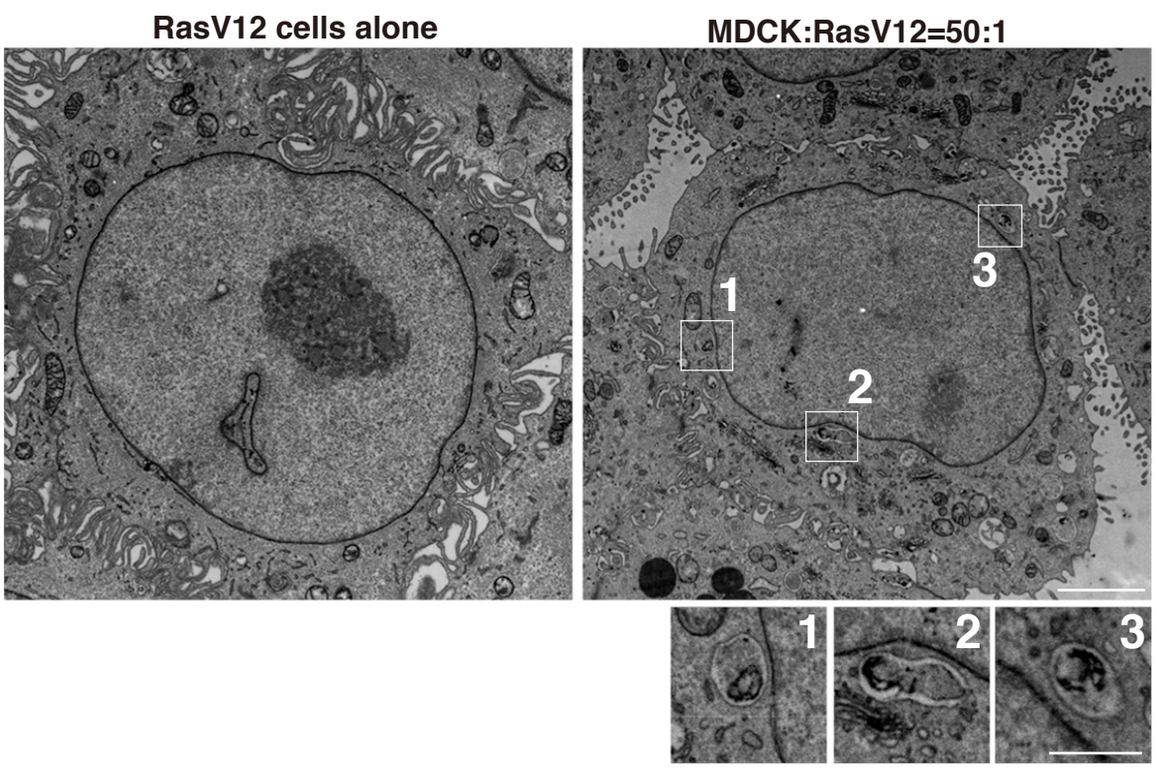

Supplementary Figure 2 Kon et al.

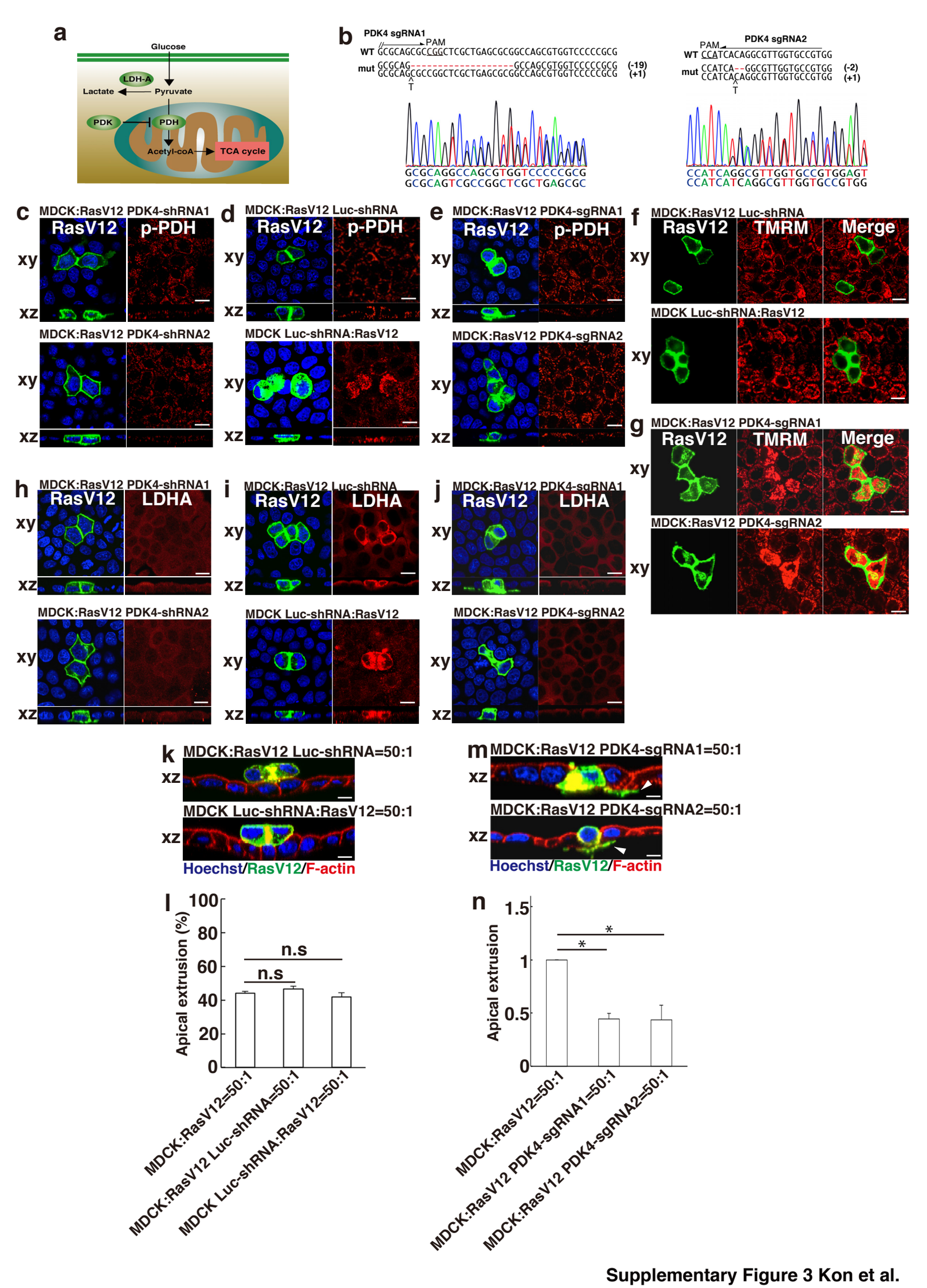

Supplementary Figure 3 Kon et al.

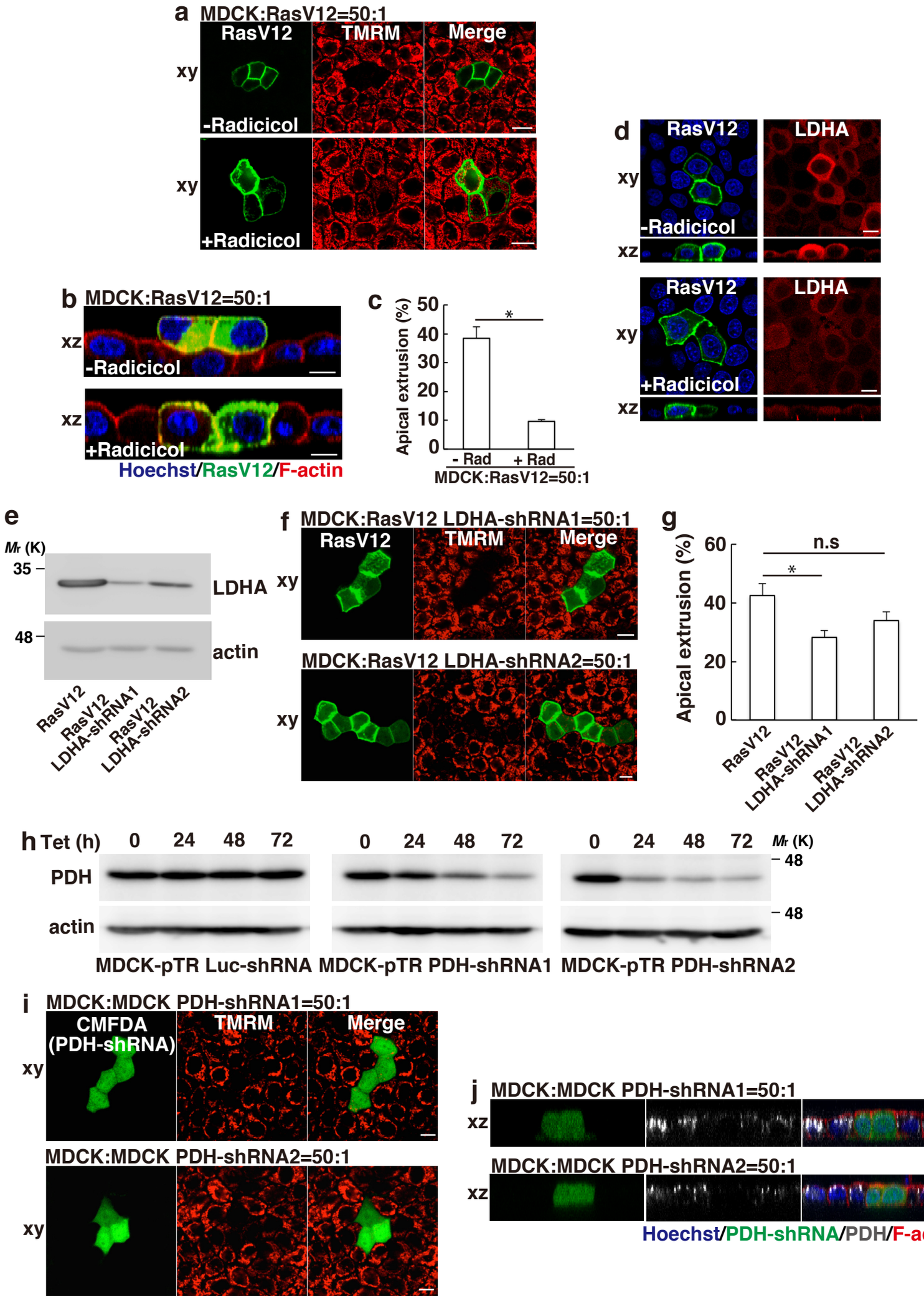

Supplementary Figure 4 Kon et al.

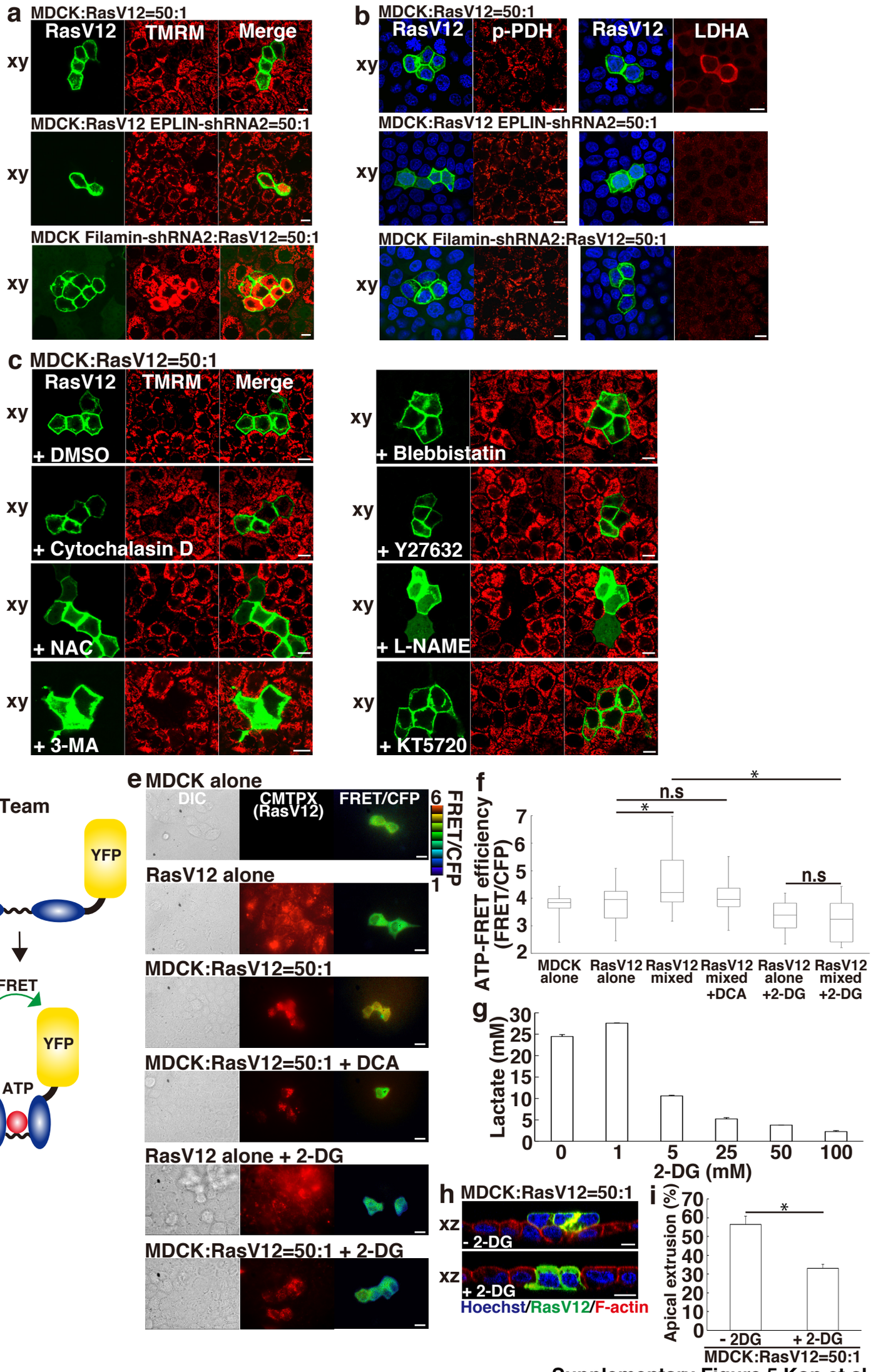

Supplementary Figure 5 Kon et al.

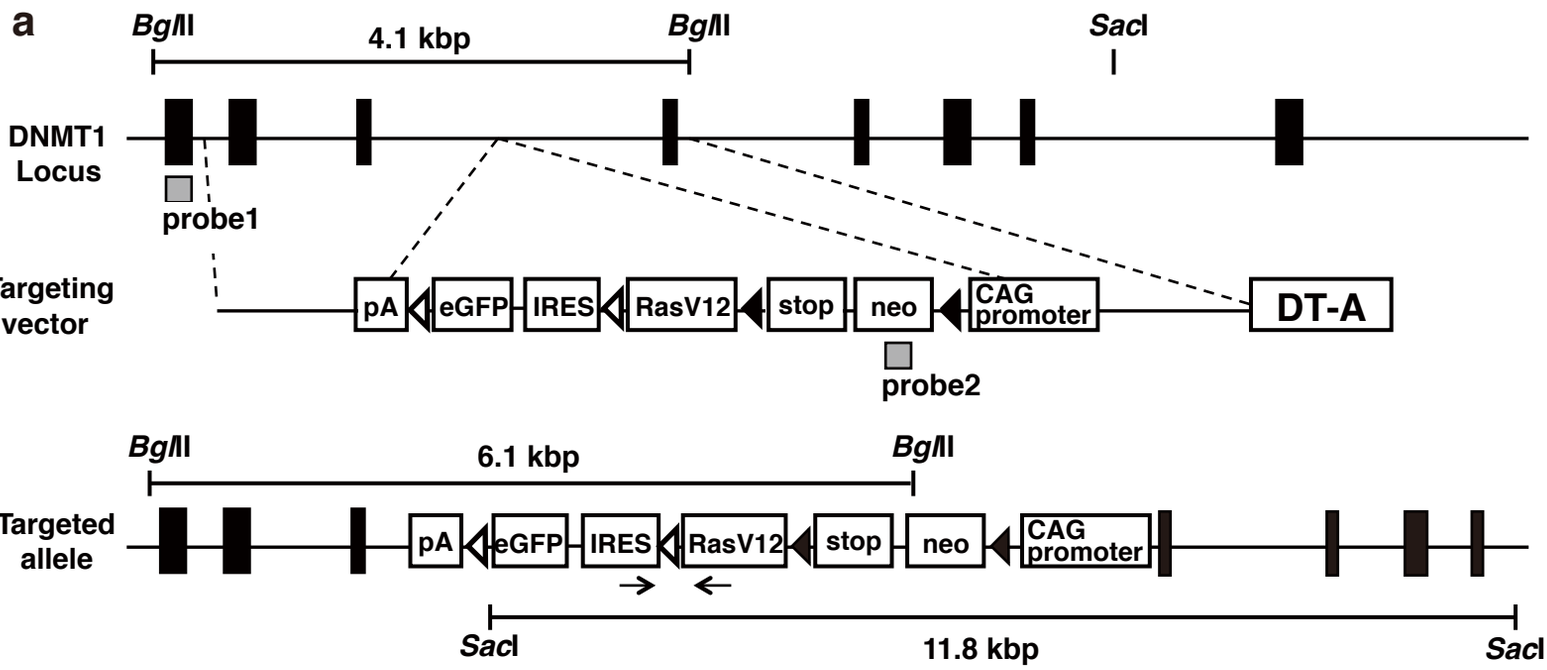

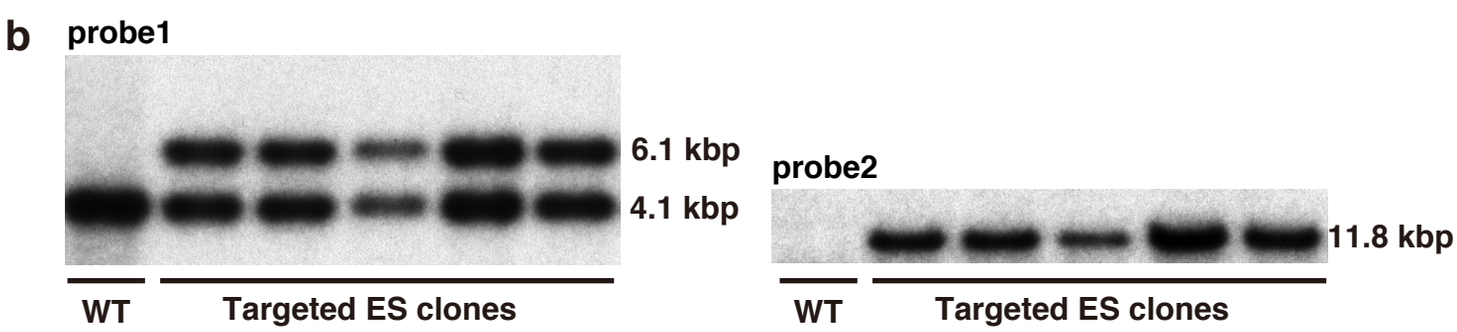

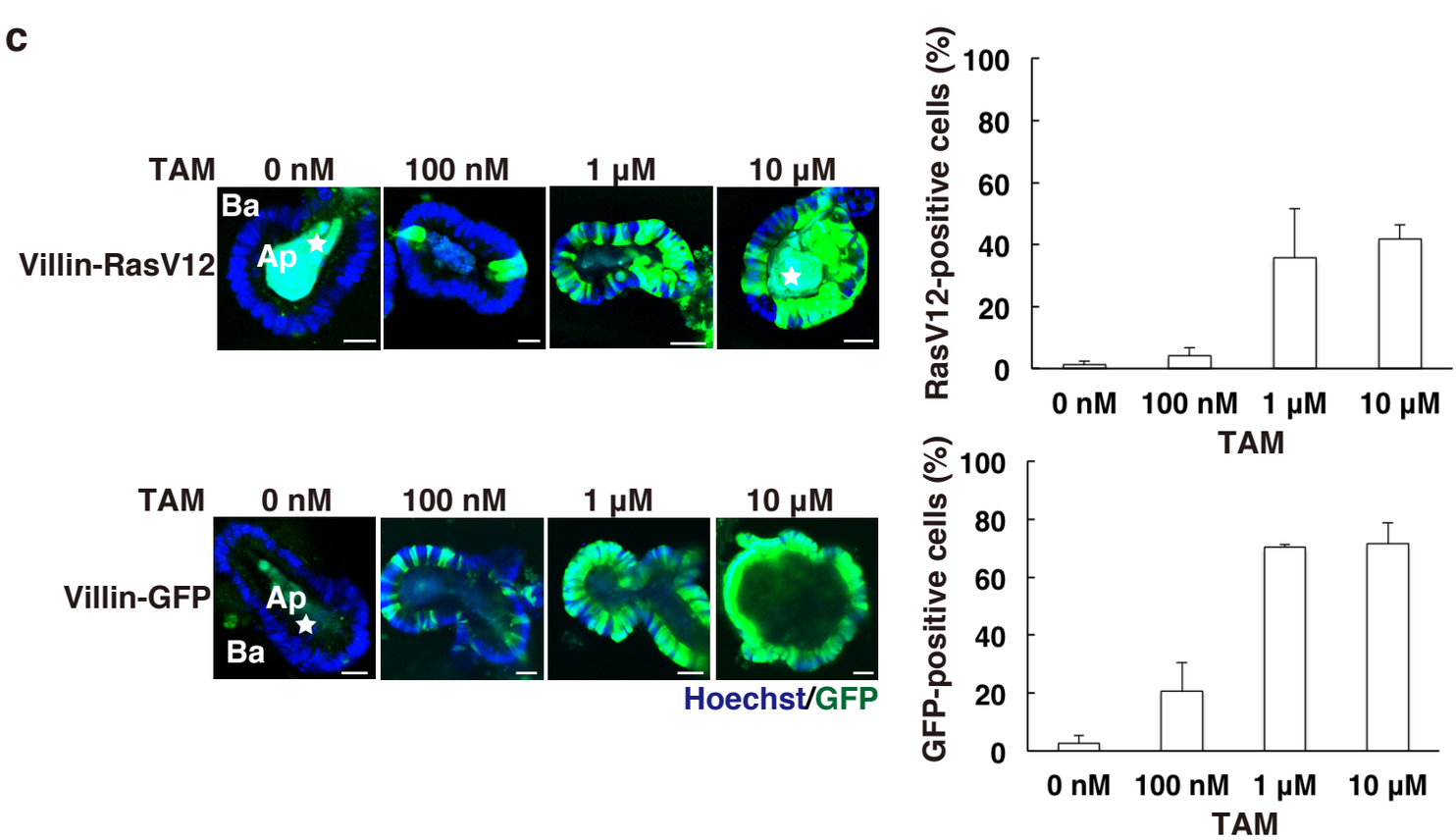

Supplementary Figure 6 Kon et al.

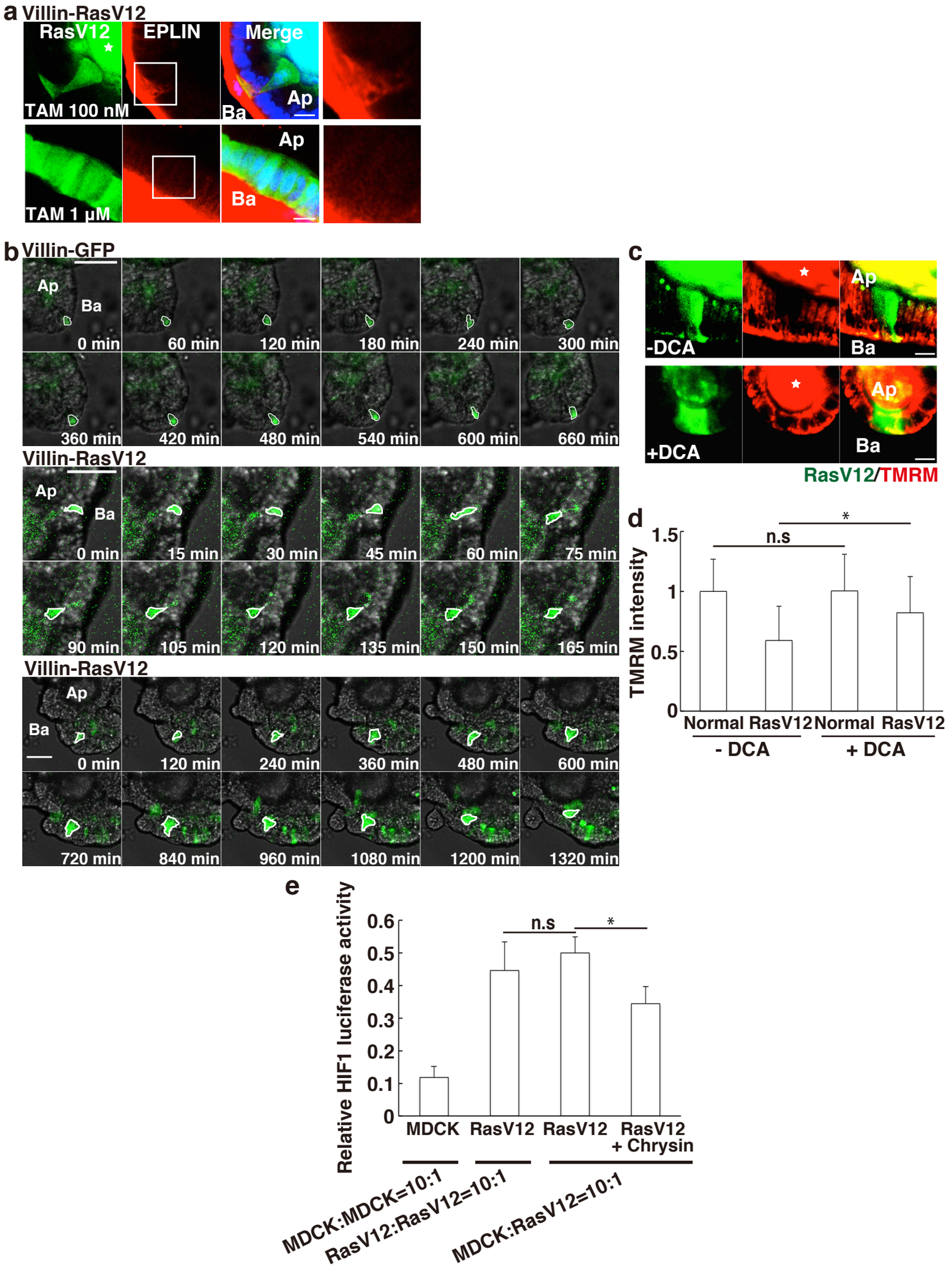

Supplementary Figure 7 Kon et al.

a

Inhibitor	Target	Extrusion	TMRM incorporation
Blebbistatin	Myosin-Ⅱ	↓*	No effect
Cytochalasin D	Actin polymerization	↓*	No effect
Y27632	Rho kinase	↓*	No effect
NAC	ROS	No effect	No effect
L-NAME	NOS	ND	No effect
3-MA	Autophagy	↓*	No effect
KT5720	PKA	ND	↑*

b

	Conventional	EDAC-induced
Upstream regulators	HIF1, cancer-driver genes (myc, Akt, mTOR, p53)	EPLIN
Upregulated PDK	PDK1/3	PDK4
Environmental attribution	Hypoxia, Nutrients deficiency, Oxidative stress	EDAC from the neighbouring cells
Function	Cancer supportive	Cancer suppressive

c

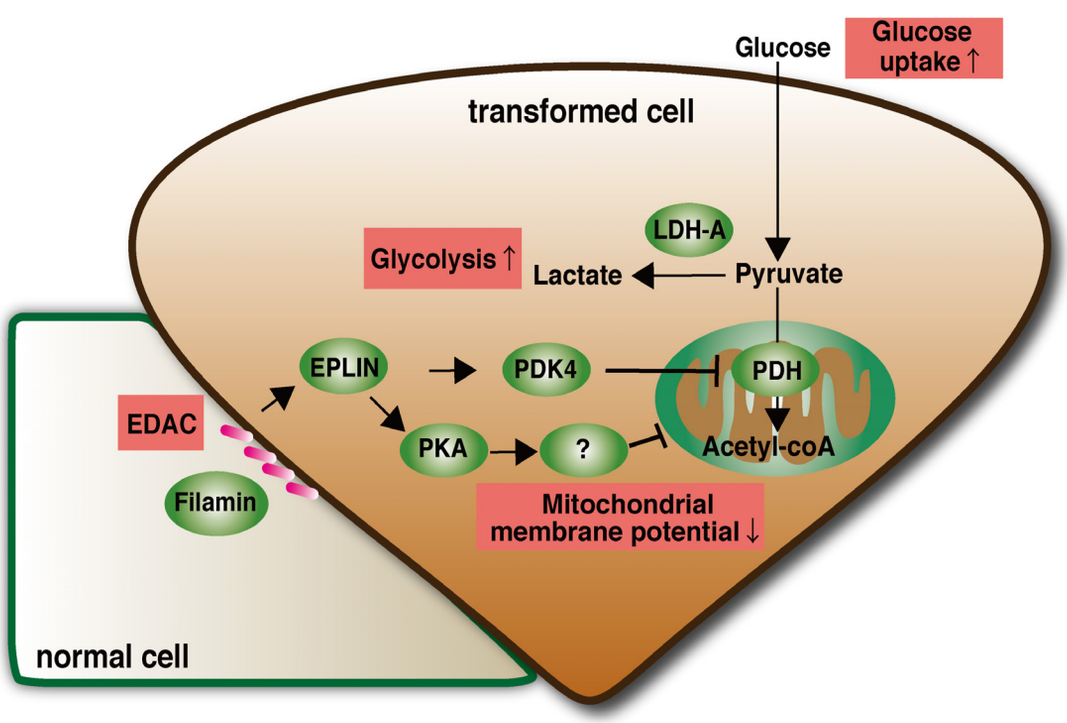

Supplementary Figure 8 Kon et al.

Fig.8i

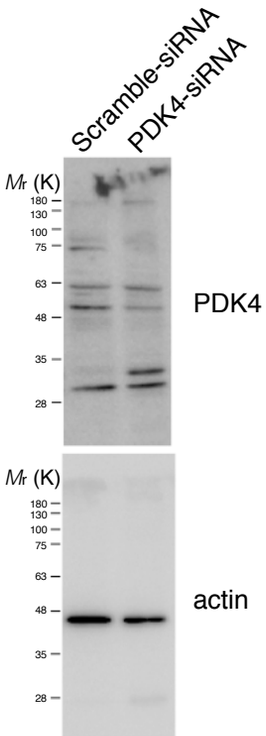

Fig.S1c

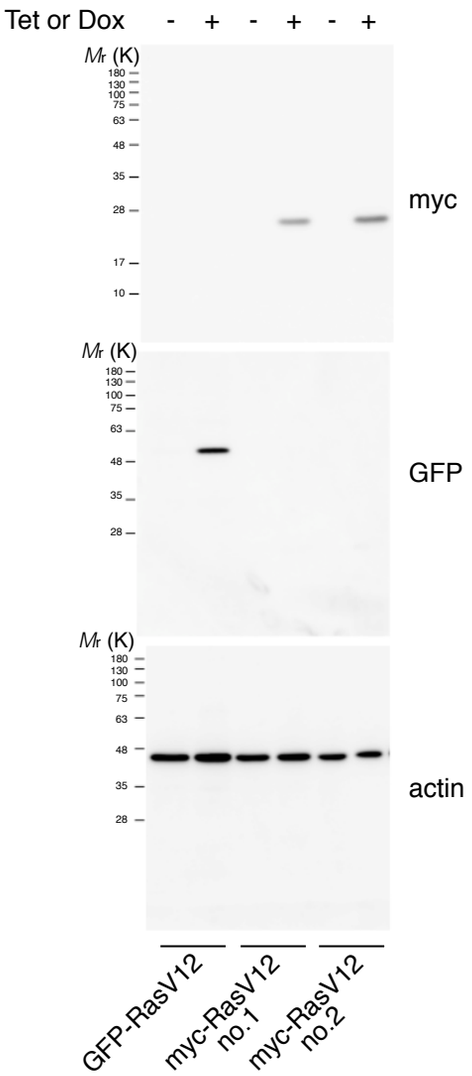

Fig.S4e

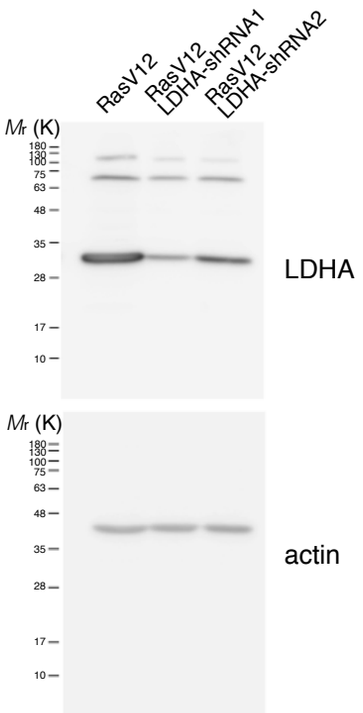

Fig.S4h

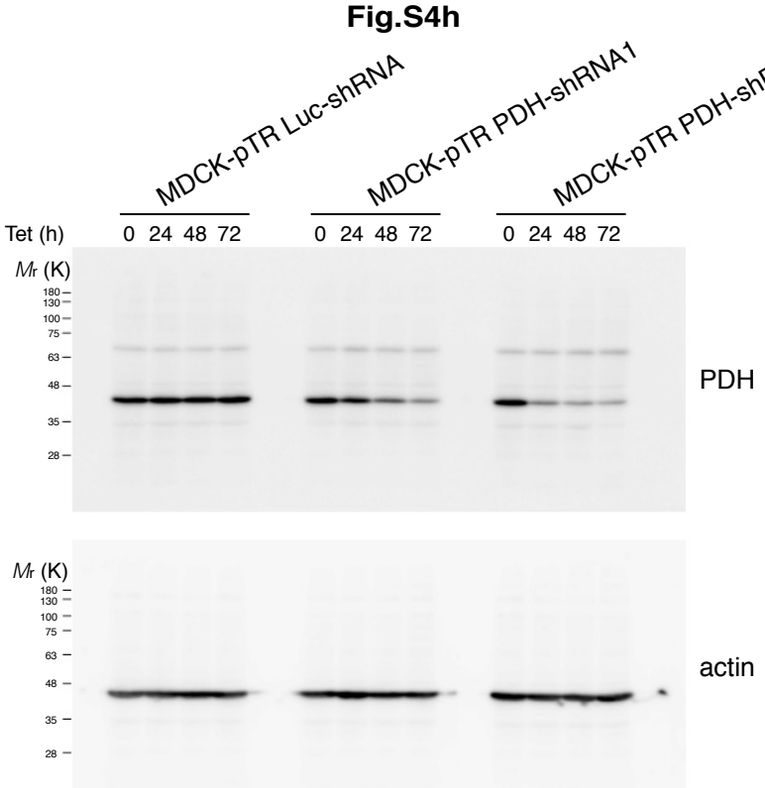

Supplementary Figure 9 Kon et al.